SIMULATIING VOLTAGE COLLAPSE DYNAMICS FOR POWER SYSTEMS WITH CONSTANT POWER LOADS

BY

SHRIRANG ABHYANKAR

DEPARTMENT OF ELECTRICAL AND COMPUTER ENGINEERING

Submitted in partial fulfillment of the
requirements for the degree of
Master of Science in Electrical Engineering
in the Graduate College of the
Illinois Institute of Technology

Approved _____
Adviser

Chicago, Illinois
December 2006

ACKNOWLEDGEMENT

I would like to take this opportunity to express my gratitude to few people without whom this thesis would not have been possible. First and foremost, I am indebted to my advisor, Dr. Alexander Flueck. The *Power System Dynamics and Stability* course I took with him triggered my interest in this topic. I am grateful to him for giving me the opportunity to work on such an exciting project in the Dynamics and Stability field. I am keenly looking forward to work on my next assignment with him in my Ph. D. years.

My parents, Mr. Gangadhar S. Abhyankar and Mrs. Sugandha G. Abhyankar, are the inspiration behind my work. I want to thank them for their constant support and encouragement.

I want to thank Dr. Shahidehpour, Dr. Emadi and Dr. Li for being members of the thesis examining committee. The courses I took with Dr. Shahidehpour and Dr. Li were a great learning experience and broadened my knowledge on Power Systems.

I want to also thank my fiancée, Archana, for bearing with me for all these years and giving me the needed emotional support and encouragement.

The discussions I had with Dr. Anurag Srivastava, Mr. Gurkan Soykan, and Mr. Cuong Nguyen, gave me different perspectives on the problem I was dealing with. I am grateful to them for sharing their views.

Finally, I want to thank God Almighty for blessing me with patience and perseverance without which everything is just dust in the wind.

TABLE OF CONTENTS

LIST OF TABLES

LIST OF FIGURES

LIST OF SYMBOLS

Symbol	Definition
V	Voltage magnitude
θ	Voltage phase angle
δ	Rotor angle
ω	Synchronous speed
E'_{qp}	Quadrature axis transient emf
E'_{dp}	Direct axis transient emf
E_{fd}	Field voltage
R_F	Rate Feedback
V_R	AVR voltage
H	Inertia Constant
X_d	Direct Axis Reactance
X'_d	Direct Axis Transient Reactance
X_q	Quadrature Axis Reactance
X'_q	Quadrature Axis Transient Reactance
T'_{d0}	Direct Axis Open Circuit transient time constant
T'_{q0}	Quadrature Axis Open Circuit transient time constant
R_s	Stator Resistance
D	Damping Constant
$\vec{V}$	Complex Bus Voltage
$\vec{I}$	Complex Current

ABSTRACT

This thesis focuses on the voltage collapse dynamics of power systems. It is well known that continuation power flow techniques can determine voltage stability limits for steady behavior of power systems. But what tools are available for transient behavior? Electromechanical Transients are studied using Transient Stability Simulators with differential-algebraic equation (DAE) models employing phasor network variables. While these simulators can follow the electromechanical transients (e.g., voltage and power swings) due to line switching with loads modeled as constant impedance, they may fail to converge for systems with constant power loads. This non-convergence has been attributed to a transient voltage collapse in the literature. However, the key issue here is that the simulation stops and the voltage collapse trajectories cannot be examined in detail. Examining the voltage collapse trajectories is important for differentiating local area collapses from widespread collapses, mitigating the sequence of events leading to a widespread cascading outage, and correctly estimating the transfer capability limit of power systems. This thesis presents a methodology for examining the voltage collapse trajectories by modeling constant power loads as voltage dependent impedance loads.

Results on a two-bus system with single phase instantaneous time domain simulation show that the voltage collapse trajectories can be examined via the proposed voltage dependent impedance load. Furthermore, the voltage dependent impedance load model has also been implemented in three phase instantaneous time domain simulation. Implementation of such a load model back in the transient stability simulation with a DAE model resolves the non-convergence problem and the voltage collapse trajectories can be tracked.

Lastly, an analysis of the non-convergence of the transient stability simulations with a DAE model for switching with constant power loads is discussed using the continuation power flow method.

CHAPTER 1

INTRODUCTION

1.1 Background

The voltage collapse issue is an important problem for electric utilities to prevent. As power systems are operated at increasing loading levels, voltage collapse becomes more likely. Today's increased loading levels are due to the fact that the system load is increasing, yet transmission line capacity is stagnant. Several constraints such as economic, environmental, and territorial issues are the cause of such a mismatch.

The traditional ways of analyzing transfer capability limits with respect to voltage collapse are based on the steady state power flow calculations. The results are expressed in the form of P-V and Q-V curves which illustrate the steady state stability limits of the system. Voltage collapse occurs immediately beyond the tip or the nose of these curves and hence these analyses are useful for prevention of steady state voltage collapse. The methods assume that the load and generation variations are small and the interconnecting transient state can be ignored. For large disturbances like tripping of transmission lines or generator outages, steady state methods reveal the pre and post-contingency equilibrium points but do not have any information about the interconnecting transient.

The transient is characterized by voltage and current swings before settling down to the operating point, assuming the system is stable. During the transient, the system can lose stability in several ways but this work focuses on voltage collapse. Transient Simulation, also referred to as Time domain integration, is typically used for analyzing the transient response of the system due to an event disturbance. The work summarized in

this thesis involves transient analysis of voltage collapse in power systems using time domain integration techniques.

1.2 Literature survey

Voltage instability incidents have been reported in power systems around the world [1], [2] and hence it becomes increasingly important to study the mechanism of voltage collapse. A survey on the literature related to voltage collapse reveals that most of the work is on steady state voltage collapse. Venikov et al. [3] were the first one to suggest a criterion for steady state voltage collapse based on sensitivity analysis. Kwanty et al. [4] applied the bifurcation analysis to the load flow equations and showed that voltage collapse occurs at a static bifurcation point. Tamura et al. [5] explained that the load flow solutions undergo saddle node bifurcation at the voltage collapse point. Since then a variety of tools such as PV and QV curve analysis, modal analysis, and sensitivity analysis methods have been proposed to estimate the steady state voltage collapse point [6]-[8].

Voltage collapse also has been explored using the system dynamics (generator models based on differential equations, excitation limits, load dynamics, tap changing transformers) [7]-[9]. In [9], the voltage collapse trajectories at the saddle node bifurcation point are captured using dynamic analysis for small load variations. A constant power load in parallel with a dynamic induction motor load is used as the load model. The dynamics of voltage collapse for line tripping considering OLTC and over-excitation limits of the generator are discussed in [10]. The load model used is an aggregate load model based on voltage exponential. In [11], an index for detecting dynamic voltage collapse is proposed.

1.3 Transient stability simulators

Dynamic analysis for a large scale power system is typically done by transient stability simulators. Traditionally, these simulators are used to observe the response of the mechanical shafts of the rotating machines after a disturbance. However, in this thesis, we are using the modeling and solution algorithm for Transient Stability to capture voltage collapse dynamics. Transient Stability of the system on events like faults, line switching, generation and load outages is determined by integrating the system equations in time. The equations describing the system are of the form

$$\begin{aligned} \dot{x} &= f(x, y, u) \\ 0 &= g(x, y) \end{aligned} \tag{1.1}$$

where, the differential equations describe the mechanical behavior of the machines and the algebraic equations are the stator current and network equations. In such a formulation, the network voltages and currents are represented using phasors. The step size used for the integration methods may vary from one millisecond to one-tenth of a second. Due to the small step size used and the extensive generator, load and other control equipment modeling done, the electromechanical transient simulation is computationally intensive compared to the static analysis methods. Examples of commercial packages are PSS/E, EUROSTAG and PowerTech TSAT.

1.4 Motivation

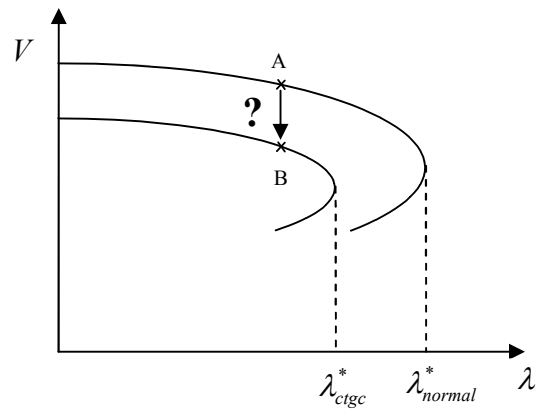

Figure1.1 Continuation power flow curves for a line outage

Figure 1.1 shows an example of PV curves for the normal case and line outage case from a continuation power flow. λ^*_{normal} is the loading limit for the system with all lines in service and λ^*_{ctgc} is the loading limit with one of the transmission lines out of service. Assume that for a given loading, the system is operating at point *A* with all the lines in service. The continuation power flow plots show that if a line is tripped then there exists a post-contingency operating point, *B*. As seen from Fig. 1.1, the system is operating at a high loading level and we want to investigate whether the system can go from point *A* to point *B* through the transient. We assume that the load is trying to absorb constant power throughout the transient.

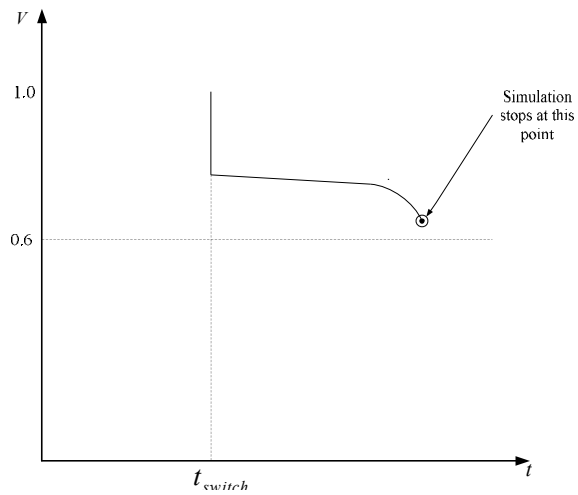

Figure 1.2 Stopping of transient stability simulation

When the transient response is analysed by a transient stability simulator, the simulation may stop due to non-convergence. As can be seen in the example plot in Figure 1.2, the voltage at which the simulation stops is above 0.6 pu. While such a stopping of the simulation has been attributed to transient voltage collapse in the literature, it still does not confirm that it is a voltage collapse. Moreover, there are some important unanswered questions left,

What is the reason for having no solution for the system?

How can the simulations be continued to follow the system trajectories?

Finding answers to these questions is the main motivation behind this thesis. While the first one answers the reason for the failure, the second one is more important for analyzing the events that may follow. The stability of the system, the operation of protective devices, the generator response, and the possibility of cascading outages are some of the critical issues that need to be answered. The voltage collapse cascade phenomenon is still a relatively unexplored domain in power system analysis. Currently, the industry predicts the potential of cascading outages based on heuristics or based on

experience. However, there is no tool that can follow the sequence of events leading to a cascade or the cascading process itself for heavily loaded systems with constant power loads.

1.5 Capturing local voltage collapse and transfer capability limit

Capturing the voltage collapse trajectories is important for differentiating local and widespread voltage collapses in large scale power systems. The static methods cannot capture local voltage collapse because the PV curves turn around at all the buses at the collapse point. The distance to steady state loading limit is also known as the *distance to collapse* and it determines the power transfer capability limit or the maximum power transfer for a given transfer direction.

In contingency ranking with respect to voltage collapse, contingencies are ranked based on their *distance to collapse*. The contingencies showing a small *distance to collapse* are ranked at the top of the contingency list and the transfer capability limit of the system corresponds to the shortest *distance to collapse*. An illustration of the above discussion is shown in Figure 1.3

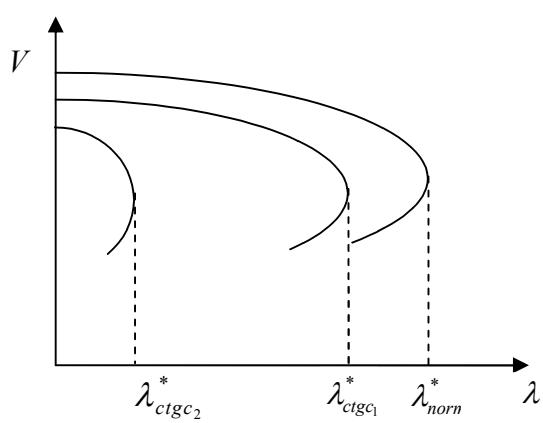

Figure 1.3 Continuation power flow curves for a system whose transfer capability limit is severely restricted by a contingency having a small *distance to collapse*

In Figure 1.3, λ^*_{normal} is the *distance to collapse* with all lines in service, $\lambda^*_{ctgc_1}$ with one of the lines out and $\lambda^*_{ctgc_2}$ corresponds to the contingency having the shortest *distance to collapse.* The contingency with a *distance to collapse* $\lambda^*_{ctgc_2}$ is ranked at the top of the contingency list and the transfer capability limit for the system is set to the post-ctgc steady state loading limit for this contingency. As seen, the transfer capability limit for the system is significantly reduced because of the small *distance to collapse*. However, if this particular contingency causes just a local voltage collapse then it is not a serious threat to the system.

If contingency 2 were to occur, the load bus experiencing the localized voltage collapse would be isolated from the system by protective devices, thereby bringing the system back to a stable operating condition with increased *distance to collapse*. Hence, identification of such local voltage collapses is necessary for properly predicting the impact of contingencies. Moreover, a better understanding of the contingency impacts will enable the industry to better measure the transfer capability limits of large scale power systems with respect to voltage collapse.

1.6 Instantaneous time domain simulators

All electrical circuits exhibit electromagnetic transients during switching. The power system with long transmission lines and various electromagnetic components exhibits very complex behavior during switching or lightning strikes. The study of this behavior is done using the electromagnetic or instantaneous time domain simulators. In the solution method, instantaneous voltage and current waveforms are used instead of phasors for analysis. The network equations are expressed in differential form along with

the differential equations for the machines. The time step ranges from 10 us to 1000 us. While instantaneous time domain simulation could be used to capture the voltage collapse dynamics, the very detailed modeling required for such studies and the time frame of interest (microseconds) are such that the computation is extremely high. Thus, even with today's powerful computers, very large portions of the power grid cannot be studied at one time for its electromagnetic behavior. In case of widespread blackouts due to cascading outages, we need to model very large regions of interconnected power systems. Examples of commercial packages are EMTP, PSCAD/EMTDC, ETAP and Power System Blockset in Simulink.

1.7 Chapter outline

Chapter 2 reviews the modeling and solution algorithms used in static voltage stability analysis of power systems. Two tools for static voltage stability analysis; power flow and continuation power flow are discussed.

The modeling and solution algorithms for Transient stability simulators are discussed in Chapter 3.

Chapter 4 describes the modeling of transmission lines and generators for instantaneous time domain simulation. The model of a load specified as constant PQ load in instantaneous time domain simulation is developed and discussed in this chapter.

Chapter 5 presents the simulations done, discussion of the results and the conclusions drawn from it.

Chapter 6 summarizes the contributions of this thesis and discusses the future work intended.

CHAPTER 2

STATIC VOLTAGE STABILITY ANALYSIS

The aim of the static methods is to find the steady state voltage stability limit of a system. The results are based on a series of power flow solutions for small disturbances. The small disturbances typically used are small variations in loading or generation. The assumption used in the static methods is that the system frequency remains constant. Under such an assumption, the total generation equals the load plus losses and hence a power flow solution can be applied for determing the stability of the system. Many contingency ranking methods are also based on the static analysis of power systems. The ranking is done by analyzing the pre-contingency and post-contingency *distance to collapse*.

The modeling of three basic elements of a power system; generators, loads and the transmission network is discussed in Section 2.1. Section 2.2 describes the solution methodologies used in two static voltage stability analysis tools; power flow and continuation power flow.

2.1 Modeling

The modeling of the various elements discussed in this section is based on the assumption that the three phase system is balanced under steady state conditions. Using this assumption, a *per phase* analysis can be done.

2.1.1 Constant power loads. Load modeling is the most critical issue in the simulation of a power system due to its diversity and composition. The net load connected to any bus comprises of a large number of diverse devices like refrigerators, heaters, pumps,

lamps, machines etc. Moreover, the load composition changes according to weather, time and economy. Hence, it is impractical to represent individual component characteristics for large scale system studies and the net load seen at substations or bulk delivery points is considered.

The estimation of the system load is done on an hourly or a daily basis to schedule the required generation. Thus, the loads are represented as constant power or constant PQ loads. These are modeled as negative power injections at the load buses.

2.1.2 Synchronous generators. Synchronous generators are the main source of electric energy in a power system. For a system to be stable, the generators in the system should operate in synchronism. The modeling of the generators from a system perspective depends on the disturbance level and the state of the power system. For steady state conditions and small disturbances, like small variations in loading or generation, the generator frequency is assumed to remain near about constant. Therefore, the dynamics of the generators are ignored and the generators are represented by their power output in static analysis. These are modeled as positive power injections at the generator buses. The generator buses are distinguished as either Slack or PV buses. The generators connected to PV buses have specified active powers and they maintain constant generator terminal voltage magnitude. These generators are assumed to have ample reactive power to support constant voltage magnitude at their terminals. However, if the generator encounters its reactive power limit then the generator voltage magnitude cannot be maintained constant and the buses are treated as PQ buses with fixed active and reactive power generation. Generators connected to slack bus pick up the extra generation and system losses. Their terminal voltage magnitude and angle is controlled to be constant.

Table 2.1 Generator bus types

Bus Type	Constant Parameters	Variable Parameters
Slack	V, θ	P_g, Q_g
PV	P_g, V	Q_g, θ

2.1.3 Transmission line network. Transmission network is the heart of a power system. Electrical power is transferred from generating stations to consumers through overhead lines and cables. The characteristics of a transmission line are determined by four parameters; series resistance R', shunt conductance G', series inductance L' and shunt capacitance C' with the parameters being per unit length parameters. These parameters are called the distributed parameters. In a line of length l, $2l$ differential equations need to be solved to describe the transmission line behavior. However, for a system analysis, the voltages and currents at the ends of the line are important. This introduces the concept of knowing the effective parameters as seen from the line ends and lumping the distributed parameters to ease the analysis. The lumped parameter representation of the line is described in this section. This type of line modeling is used for the static analysis and transient stability studies. The lumped parameter representation is valid for medium length lines. For longer lines and for more accurate representation, modeling is based on the distributed parameters itself. This distributed parameter line model is deferred to Chapter 4. The classification of lines and the associated modeling is given in Table 2.2.

Table 2.2 Line classification and modeling

Line type	Length in km.	Modeled by
Short	$l < 80$	Series impedance
Medium	$80 < l < 200$	Nominal pi model
Long	$l > 200$	Equivalent Pi Model, Distributed parameter line

If l is the length of the line, $z \equiv r + jx$ is the series impedance per unit length and $y \equiv g + jb$ is the shunt admittance per unit length, then by multiplying these parameters by the line length a nominal lumped parameter model is obtained. For long transmission lines or for better accuracy, an equivalent lumped parameter model is used instead of nominal lumped parameter model. The equivalent lumped parameter model is based on the characteristic impedance, Z_C, propagation constant, γ, and the line length. Typically, the shunt conductance of transmission lines is very small and is ignored.

These lumped parameters can be connected in a π or a T configuration to model the transmission line. The π model is the preferred choice of transmission line model in static analysis and transient stability simulators with a DAE model. Figure 2.1 shows the π model of a transmission line. The sending end and the receiving end voltage, current expressions can be related by equation (2.1) as

$$\begin{bmatrix} \vec{I}_S \\ \vec{I}_R \end{bmatrix} = \begin{bmatrix} Y + jB/2 & -Y \\ -Y & Y + jB/2 \end{bmatrix} \begin{bmatrix} \vec{V}_S \\ \vec{V}_R \end{bmatrix} \tag{2.1}$$

In compact form, (2.1) can be written as $\vec{I} = \vec{Y}\vec{V}$

For a nominal pi model,

$$Y \equiv yl\ ,$$

$$B \equiv bl\ .$$

For an equivalent pi model,

$$Y \equiv \frac{1}{Z_C \sinh \gamma l}\ ,$$

$$B \equiv \frac{2 \tanh \gamma l / 2}{Z_C}$$

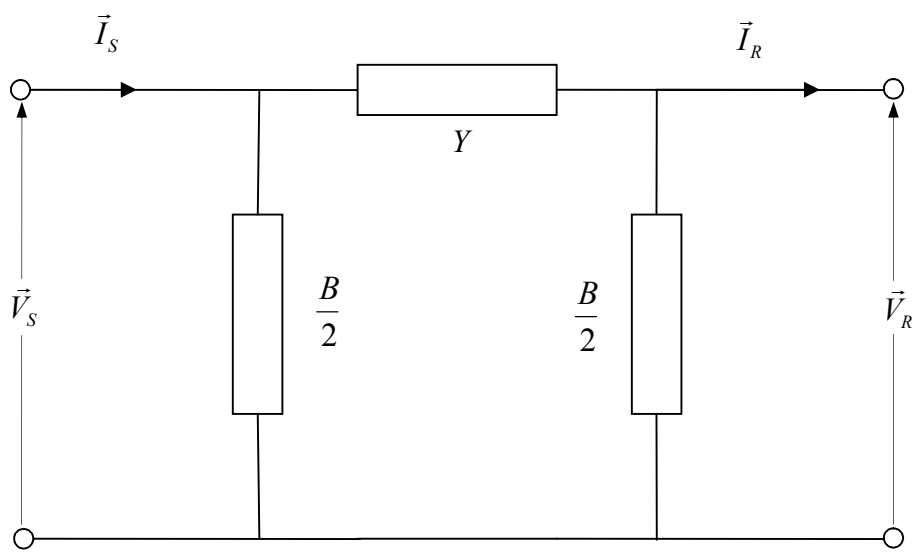

Figure 2.1 π Model of a transmission line

2.2 Solution methods

This section discusses the solution methods for power flow, continuation power flow. Both these methods are used for the steady state analysis of power systems.

2.2.1 Power flow. A power flow finds the steady state operating point for the power system. It solves for the bus voltage magnitudes and phase angle, reactive powers and

voltage phase angles at generator buses. Studies involving power flow include slow variation of loads over an hour, day etc or planning studies. During such studies, the load is assumed as constant PQ because the load is fixed for a particular time. Power flows are also used for initializing the transient stability simulations. The solution methodology is discussed in the succeeding paragraphs.

Given a power system with N buses, the complex voltage at bus k can be represented as

$$\vec{V}_k = E_k + jF_k = V_k e^{j\theta_k} \qquad k = 1,\ldots,N$$

The complex power injection into bus k can be represented as

$$S_k^{inj} \equiv P_k^{inj} + jQ_k^{inj} \qquad k = 1,\ldots,N$$

The real power injection can be represented in terms of real power generator and load respectively

$$P_k^{inj} = P_k^G + jQ_k^D$$

The series complex admittance between bus k and l can be represented as

$$Y_{kl} \equiv G_{kl} + jB_{kl} \qquad k = 1,\ldots,N$$

The sum of all the complex admittance connected to bus k can be represented as

$$Y_{kk} \equiv G_{kk} + jB_{kk} \qquad k = 1,\ldots,N$$

The power system admittance matrix, called y_{bus}, is built by Y_{kl} and Y_{kk}. The power flow equations can be stated via the principle of complex power conversion.

The specific complex power injection into bus k, applying can be represented as

$$\vec{S}_k^{inj} = \vec{V}_k \vec{I}_k^*$$

$$= \vec{V}_k \sum_{l=1}^{N} (\vec{Y}_{kl}\vec{V}_l)^*$$

$$= V_k e^{j\theta_k} \sum_{l=1}^{N} (G_{kl} - jB_{kl}) V_l e^{-j\theta_l}$$

$$= V_k \sum_{l=1}^{N} V_l (G_{kl} - jB_{kl}) e^{j(\theta_k - \theta_l)}$$

Separating into its real and imaginary parts from the above equation, the real power equation has the real injection into bus *k*, labeled P_k^{inj}, on the left hand side and the real power flow out of bus *k* on the right hand side. The reactive power equation has the reactive injection into bus *k*, labeled Q_k^{inj}, on the left hand side and the reactive power flow out of bus *k* on the right hand side,

$$P_k^{inj} = |V_k| \sum_{l=1}^{N} |V_l| [(G_{kl} \cos(\theta_k - \theta_l) + B_{kl} \sin(\theta_k - \theta_l)] \tag{2.2}$$

$$Q_k^{inj} = |V_k| \sum_{l=1}^{N} |V_l| \ [G_{kl} \sin(\theta_k - \theta_l) - B_{kl} \cos(\theta_k - \theta_l)] \tag{2.3}$$

The real and reactive power flow at bus *k* can be written as

$$P_k^{inj} = |V_k| \sum_{l=1}^{N} |V_l| [(G_{kl} \cos(\theta_{kl}) + B_{kl} \sin(\theta_{kl})] \tag{2.4}$$

$$Q_k^{inj} = |V_k| \sum_{l=1}^{N} |V_l| [G_{kl} \sin(\theta_{kl}) - B_{kl} \cos(\theta_{kl})] \tag{2.5}$$

where $\theta_{kl} = \theta_k - \theta_l$

In equations (2.4) and (2.5), the unknowns are the voltage magnitudes, phase angles and generator powers. Thus, there are 2*n* equations and 4*n* unknowns. Also, the *y*bus matrix for the entire system is singular. To get a solution for the system, some of the parameters are fixed and the buses classified accordingly. The classification of the buses is given in Table 2.3

Table 2.3 Classification of network buses

Bus Type	Constant Parameters	Variable Parameters
Slack	V, θ	P_g, Q_g
PV	P_g, V	Q_g, θ
PQ	P_d, Q_d	V, θ

By classifying the buses into different categories and fixing the variables, the number of unknowns equals the number of equations and the system can be solved.

2.2.2 Continuation power flow. Continuation methods or branch tracing methods are used to trace a curve given an initial point on the curve. These are also called as predictor-corrector methods since they involve the prediction of the next solution point and correcting the prediction to get the next point on the curve. The continuation process can be diagrammatically shown as given below:

$$(x^j, \lambda^j) \xrightarrow{\text{Predictor}} (\hat{x}^{j+1}, \hat{\lambda}^{j+1}) \xrightarrow{\text{Corrector}} (x^{j+1}, \lambda^{j+1})$$

where, (x^j, λ^j) represents the current solution, $(\hat{x}^{j+1}, \hat{\lambda}^{j+1})$ is the predicted solution and (x^{j+1}, λ^{j+1}) is the next solution on the curve.

Consider a system of n nonlinear equations $f(x) = 0$ and n unknowns $x_i, i = 1:n$. By adding a controlling variable λ and one more equation to the system, x can be traced by varying λ. λ is called the continuation parameter. The resulting system $f(x, \lambda) = 0$ has $n + 1$ dimensions and has $n + 1$ unknowns. The additional equation is a parameterized

equation which identifies the location of the current solution with respect to the previous or next solution. The different kinds of parameterization used are

- Physical Parameterization: using the controlling parameter λ itself, in which case the step length is $\Delta\lambda$. While this parameter has the advantage of having physical significance, it encounters difficulties at turning points.
- Local Parameterization: uses either the controller parameter λ or any component $x_i, i = 1:n$. The step length in this case is Δx_i or $\Delta\lambda$.
- Arc Length Parameterization: employs arc length along the solution curve to perform parameterization, the step length in that case being $\Delta\gamma$

$$\Delta\gamma = \sqrt{\{\sum_{i=1}^{n}(x_i - x_i(\gamma))^2 + (\lambda - \lambda(\gamma))^2\}}$$

All the above parameterizations can be used as the additional equation $p(x,\lambda) = 0$, to formulate an extended system having $n + 1$ equations.

The predictor is used for predicting the next solution. The better the prediction, the faster is the convergence to the solution point. Tangent predictors are one of the types of predictors used in continuation methods. They give a very good approximation to the next solution point if the curve is nearly flat. If (x^j, λ^j) is the current solution, then the tangent to the curve is given by $\nabla f(x^j, \lambda^j)$. Once the gradient is found, the next step is to find the magnitude and the direction of the unique tangent vector. The tangent vector is given by the solution of the linear system given in equation 2.6

$$\begin{bmatrix} \nabla f(x^j, \lambda^j) \\ u^T \end{bmatrix} z = \begin{bmatrix} 0 \\ 1 \end{bmatrix} \tag{2.6}$$

u is an n + 1 dimensional vector with all elements equal to zero, except n + 1 element.. Norm two normalization is further done to normalize the unique tangent vector z . The approximation $(\hat{x}^{j+1}, \hat{\lambda}^{j+1})$ for the next solution (x^{j+1}, λ^{j+1}) is given by

$$(x^{j+1}, \lambda^{j+1}) = (x^{j}, \lambda^{j}) + \sigma z \tag{2.7}$$

Once the predictor gives an approximation $(\hat{x}^{j+1}, \hat{\lambda}^{j+1})$, the error must be corrected to get the next solution (x^{j+1}, λ^{j+1}). Newton's method is widely used for the solution of the nonlinear system due to its fast convergence property and can be used as a corrector.

Continuation methods are used in power systems to determine the steady state stability limit. The limit is determined from a nose curve where the nose represents the maximum power transfer that the system can handle given a power transfer schedule. The power flow equations are modeled as

$$g(x) = \begin{bmatrix} P(x) - P^{inj} \\ Q(x) - Q^{inj} \end{bmatrix} = 0 \tag{2.7}$$

here $x \equiv (V_i, \theta_i) \qquad i = 1, ..., N$.

To determine the steady state limit, the power flow equations are restructured as

$$f(x, \lambda) \equiv g(x) - \lambda b \tag{2.8}$$

where b is the vector of power transfer given as

$$b \equiv \begin{bmatrix} \hat{P}^{inj} - P^{inj} \\ \hat{Q}^{inj} - Q^{inj} \end{bmatrix}$$

The effects of the variation of loading or generation can be investigated using the continuation method by formulating the b vector appropriately.

CHAPTER 3

TRANSIENT STABILITY SIMULATORS

Static Analysis gives a measure of the steady state voltage stability limits of the power system. However for events such as line outages, these methods only determine the equilibrium of the pre-contingency and post-contingency states but do not give any information about the transient i.e., the connecting transient state between the two steady states is completely ignored. A voltage collapse can occur during the transient following a contingency and the transient response needs to be examined. One way of analyzing the transient is by observing the system trajectories in time. Transient Stability Simulators with a DAE model is the preferred choice for such a time domain analysis. These simulators are also called electromechanical transients simulators as they are typically used for assessing the transient stability of generators. Electromechanical transients simulators use algebraic power flow equations for the network quantities and differential equations governing the generator dynamics. This differential algebraic model, abbreviated as DAE, and its solution methodology are discussed in this chapter. These equations are from [12] which has a detailed description of Transient Stability Simulation.

3.1 Differential-algebraic model

The differential-algebraic equations for an *m* machine, *n* bus system with a the IEEE type I exciter model are given as

3.1.1 Differential equations. The differential equations for a detailed two-axis generator models at *m* buses are

$$\frac{d\delta_i}{dt} = \omega_i - \omega_s \tag{3.1}$$

$$\frac{2H_i}{\omega_s}\frac{d\omega_i}{dt} = T_{Mi} - E'_{di}I_{di} - \left(X'_{qi} - X'_{di}\right)I_{di}I_{qi} - D_i\left(\omega_i - \omega_s\right) \tag{3.2}$$

$$T'_{doi}\frac{dE'_{qi}}{dt} = -E'_{qi} - \left(X_{di} - X'_{di}\right)I_{di} + E_{fdi} \tag{3.3}$$

$$T'_{qoi}\frac{dE'_{di}}{dt} = -E'_{di} + \left(X_{qi} - X'_{qi}\right)I_{qi} \tag{3.4}$$

$$T_{Ei}\frac{dE_{fdi}}{dt} = -\left(K_{Ei}E_{fdi} + S_{Ei}\left(E_{fdi}\right)\right) + V_{Ri} \tag{3.5}$$

$$T_{Fi}\frac{dR_{fi}}{dt} = -R_{fi} + \frac{K_{Fi}}{T_{Fi}}E_{fdi} \tag{3.6}$$

$$T_{Ai}\frac{dV_{Ri}}{dt} = -V_{Ri} + K_{Ai}R_{fi} - \frac{K_{Ai}K_{Fi}}{T_{Fi}}E_{fdi} + K_{Ai}\left(V_{refi} - V_i\right) \tag{3.7}$$

where $i = 1,...,m$

These equations are for a two-axis machine model with saturation, subtransient reactances and the stator transients neglected. The governor dynamics are also not modeled resulting in constant mechanical torque input. The limit constraints on the voltage regulator output are also neglected. A linear damping term is assumed for the friction and windage torque. Equations (3.1)-(3.4) represent the generator dynamics while (3.5)-(3.7) represent the exciter dynamics.

3.1.2 Stator algebraic equations. The stator algebraic equations follow the dynamic equivalent circuit given in Fig. 3.1. Application of KVL yields the stator algebraic equations:

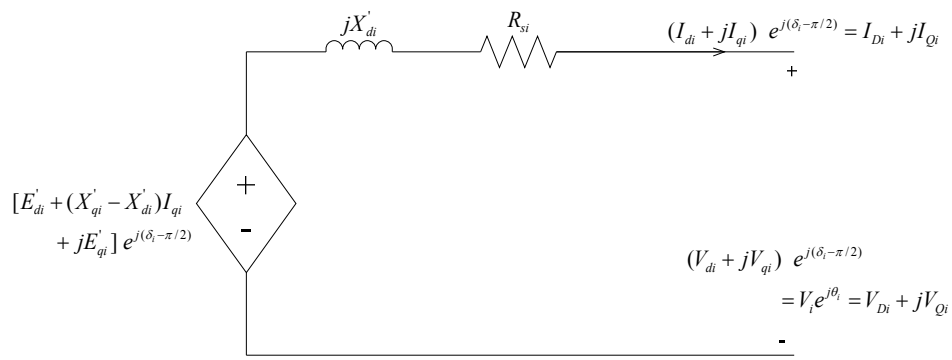

Figure 3.1 Synchronous machine two-axis model dynamic *circuit* (i = 1,…, m)

$$0 = V_i e^{j\theta_i} + (R_{si} + jX'_{di})(I_{di} + jI_{qi})e^{j(\delta_i - \frac{\pi}{2})} - [E'_{di} + (X'_{qi} - X'_{di})I_{qi} + jE'_{qi}]e^{j(\delta_i - \frac{\pi}{2})} \qquad (3.8)$$
$$i = 1,...,m$$

3.1.3 Network equations. The network equations at the n buses are written as

For generator buses,

$$V_i e^{j\theta_i}(I_{di} - jI_{qi})e^{-j(\delta_i - \frac{\pi}{2})} + P_{Li}(V_i) + jQ_{Li}(V_i) = \sum_{k=1}^{n} V_i V_k Y_{ik} e^{j(\theta_i - \theta_k - \alpha_{ik})} \qquad (3.9)$$
$$i = 1,.....,m$$

For load buses,

$$P_{Li}(V_i) + jQ_{Li}(V_i) = \sum_{k=1}^{n} V_i V_k Y_{ik} e^{j(\theta_i - \theta_k - \alpha_{ik})} \qquad i = m+1,.....,n \qquad (3.10)$$

Equations (3.9) and (3.10) represent the reactive power balance at the generator and the load buses. In equation (3.9), $V_i e^{j\theta_i}(I_{di} - jI_{qi})e^{-j(\delta_i - \frac{\pi}{2})} \triangleq P_{Gi} + jQ_{Gi}$ represents the complex power injected into the bus by generator i.

3.1.4 System dimensions and variables. The resultant model comprises of

- Seven differential equations for each machine i.e 7m differential equations
- One complex stator algebraic equation for each machine or *2m* real equations.

- One complex network equation at each network buses or 2*n* real equations.

The total number of equations to be solved is 7*m* + 2*m* + 2*n*. The state and the algebraic variables are

- $x_i \equiv [\delta_i, \omega_i, E'_{qi}, E'_{di}, E_{fdi}, R_{fi}, V_{Ri}]$ $\quad i = 1,...m$
- $I_{dqi} \equiv [I_{di}, I_{qi}]$ $\quad i = 1,...m$
- $\overline{V} \equiv [V_i, \theta_i]$ $\quad i = 1,...n$

3.2 DAE model representation and numerical solution methods

The DAE model discussed in the last section can be represented in power balance or current balance form depending on how the network equations are represented. Power balance form uses the polar form for the network variables whereas the current balance form uses the rectangular form. The current balance form is more popular in the industry.

3.2.1 Power balance form. On separating the network equations (3.9) and (3.10) into real and imaginary parts, we get the following equations

$$I_{di}V_i \sin(\delta_i - \theta_i) + I_{qi}V_i \cos(\delta_i - \theta_i) + P_{Li}(V_i) - \sum_{k=1}^{n} V_i V_k Y_{ik} \cos(\theta_i - \theta_k - \alpha_{ik}) = 0 \qquad i = 1,...,m \tag{3.11}$$

$$P_{Li}(V_i) - \sum_{k=1}^{n} V_i V_k Y_{ik} \cos(\theta_i - \theta_k - \alpha_{ik}) = 0 \qquad i = m+1,...,n \tag{3.12}$$

$$I_{di}V_i \cos(\delta_i - \theta_i) - I_{qi}V_i \sin(\delta_i - \theta_i) + Q_{Li}(V_i) - \sum_{k=1}^{n} V_i V_k Y_{ik} \sin(\theta_i - \theta_k - \alpha_{ik}) = 0 \qquad i = 1,...,m \tag{3.13}$$

$$Q_{Li}(V_i) - \sum_{k=1}^{n} V_i V_k Y_{ik} \sin(\theta_i - \theta_k - \alpha_{ik}) = 0 \qquad i = m+1,...,n \tag{3.14}$$

Equations (3.11) and (3.12) represent the real power balance equations at each buses while equations (3.13) and (3.14) represent the reactive power balance equations at the buses.

The stator algebraic equations are represented in the polar form as given in equation (3.15)

$$\begin{bmatrix} I_{di} \\ I_{qi} \end{bmatrix} = \left[Z_{d-q,i} \right]^{-1} \begin{bmatrix} E'_{di} - V_i \sin\left(\delta_i - \theta_i\right) \\ E'_{qi} - V_i \cos\left(\delta_i - \theta_i\right) \end{bmatrix} \qquad i = 1,\ldots,m \tag{3.15}$$

Along with the differential equations for the generator, the DAE model can be symbolically represented as

$$\dot{x} = f_o\left(x, I_{dq,} \overline{V}, u\right) \tag{3.16}$$

$$I_{dq} = h\left(x, \overline{V}\right) \tag{3.17}$$

$$0 = g_o\left(x, I_{d-q,} \overline{V}\right) \tag{3.18}$$

The network variables are represented in polar form with the voltage magnitude V_i and the phase angle θ_i as the variables at each bus.

To find the solution for the DAE system, the differential equations are integrated from time t_n to t_{n+1} using the trapezoidal rule while solving the algebraic equations at t_{n+1}. The resulting equations to be solved are in form given in equations (3.19)-(3.21)

$$[x_{n+1} - \frac{\Delta t}{2} f_0(x_{n+1}, I_{dq,n+1}, \overline{V}_{n+1}, u_{n+1})] - [x_n + \frac{\Delta t}{2} f_0(x_n, I_{dq,n}, \overline{V}_n, u_n) = 0 \tag{3.19}$$

$$I_{dq,n+1} - h(x_{n+1}, \overline{V}_{n+1}) = 0 \tag{3.20}$$

$$g_0(x_{n+1}, I_{dq,n+1}, \overline{V}_{n+1}) = 0 \tag{3.21}$$

At each time step, equations (3.19)-(3.21) are solved by Newton's method to obtain the state and the algebraic variables.

3.2.2 Current balance form. The current balance form expresses the network equations in the form $\overline{I} = \overline{Y}_N \overline{V}$ where $\overline{Y}_N$ is the *y*bus matrix, $\overline{I}$ is the current injection vector and $\overline{V}$ is the voltage vector. The system equations are obtained by dividing equations (3.9) and (3.10) by the complex voltage and then taking the complex conjugate.

$$\left(I_{di} + jI_{qi}\right)e^{j\left(\delta_i - \pi/2\right)} + \frac{P_{Li}\left(V_i\right) - jQ_{Li}\left(V_i\right)}{V_i e^{-j\theta_i}} = \sum_{k=1}^{n} Y_{ik} e^{j\alpha_{ik}} V_k e^{j\theta_k} \qquad i = 1 \ldots, m \tag{3.22}$$

$$\frac{P_{Li}\left(V_i\right) - jQ_{Li}\left(V_i\right)}{V_i e^{-j\theta_i}} = \sum_{k=1}^{n} Y_{ik} e^{j\alpha_{ik}} V_k e^{j\theta_k} \qquad i = m+1, \ldots, n \tag{3.23}$$

For the solution of the DAE system, representation of the network variables and equations in the rectangular form provides computational ease for solving equations (3.22) and (3.23). Accordingly, the network equations can be symbolically represented as

$$I^e(x, I_{dq}, V^e) = Y_N^e V^e \tag{3.24}$$

where, $I_i^e \equiv [I_{Di}, I_{Qi}]$, $V_i^e \equiv [V_{Di}, V_{Qi}]$ for $i = 1, \ldots, n$. The algebraic stator equations are expressed to adapt to the form of network variables as

$$\begin{bmatrix} I_{di} \\ I_{qi} \end{bmatrix} = \left[Z_{d-q,i}\right]^{-1} \begin{bmatrix} E'_{di} \\ E'_{qi} \end{bmatrix} - \left[Z_{d-q,i}\right]^{-1} \begin{bmatrix} \sin\delta_i & -\cos\delta_i \\ \cos\delta_i & \sin\delta_i \end{bmatrix} \begin{bmatrix} V_{Di} \\ V_{Qi} \end{bmatrix} = h_{ri}\left(x_i, V_{Di}, V_{Qi}\right) \tag{3.25}$$

Further, the generator state variables and the stator algebraic variables are grouped together to form a new vector $X_i \equiv [x_i, I_{dqi}]$ and equations (3.19)-(3.20) are grouped as

$$F_M(X_{n+1}, V_{n+1}^e, u_{n+1}, X_n, V_n^e, u_n) = 0 \tag{3.26}$$

The network equations to be solved at t_{n+1} time instant in the form

$$I^e(x_{n+1}, I_{dq,n+1}, V^e_{n+1}) = Y^e_N V^e_{n+1} \tag{3.27}$$

Equations (3.26) and (3.27) are solved using the Newton method with the network variables solved for first followed by the solution for the state and the stator algebraic variables. This process is carried out for each time step.

3.3 Disturbance simulation

Typical large disturbances include faults on the network, line trippings, generator outages, load outages etc. Such disturbances are very fast compared to the generator dynamics which have large mechanical time constants. The stator equations are also algebraic equations and hence respond instantaneously to the disturbance. Hence, the network and the stator algebraic variables are solved at the disturbance time to reflect the post-disturbance values. This one additional solution at the disturbance time involves the solution of the equations

$$I_{dq}(t_d+) = h^f\left(x(t_d), \overline{V}(t_d+)\right) \tag{3.28}$$

$$0 = g^f\left(x(t_d), I_{dq}(t_d+), \overline{V}(t_d+)\right) \tag{3.29}$$

where the superscript *f* indicates that the algebraic equations correspond to the faulted state and t_d represents the fault time. With the post-disturbance algebraic solution thus obtained, the trapezoidal integration process is again resumed.

3.4 Initialization

To start the transient stability simulation in steady state, the network, stator algebraic and dynamic variables need to be initialized. A power flow solution is used to

obtain the steady state operating point for the network variables. Using the power flow solution, the initial values for the dynamic variables are obtained by setting all the derivative terms to zero. The initialization of the dynamic variables and the stator algebraic variables is discussed in detail in [12].

3.5 Flowchart for transient stability simulation

The flow chart shown in Fig. (3.2) has the the network equations in the power balance form. One extra solution, as denoted by the state *A*, is carried out to reflect the instantaneous network and stator current response to the disturbance. Fig. (3.3) shows the flowchart for finding out the solution for state *A*. The same flowchart can be used for the current balance form by restructuring the network equations. However, in each iteration of the Newton method, the network variables are solved for first followed by the solution of the state and the stator algebraic variables. The convergence of the Newton iterations is checked for the solution of equation (3.26).

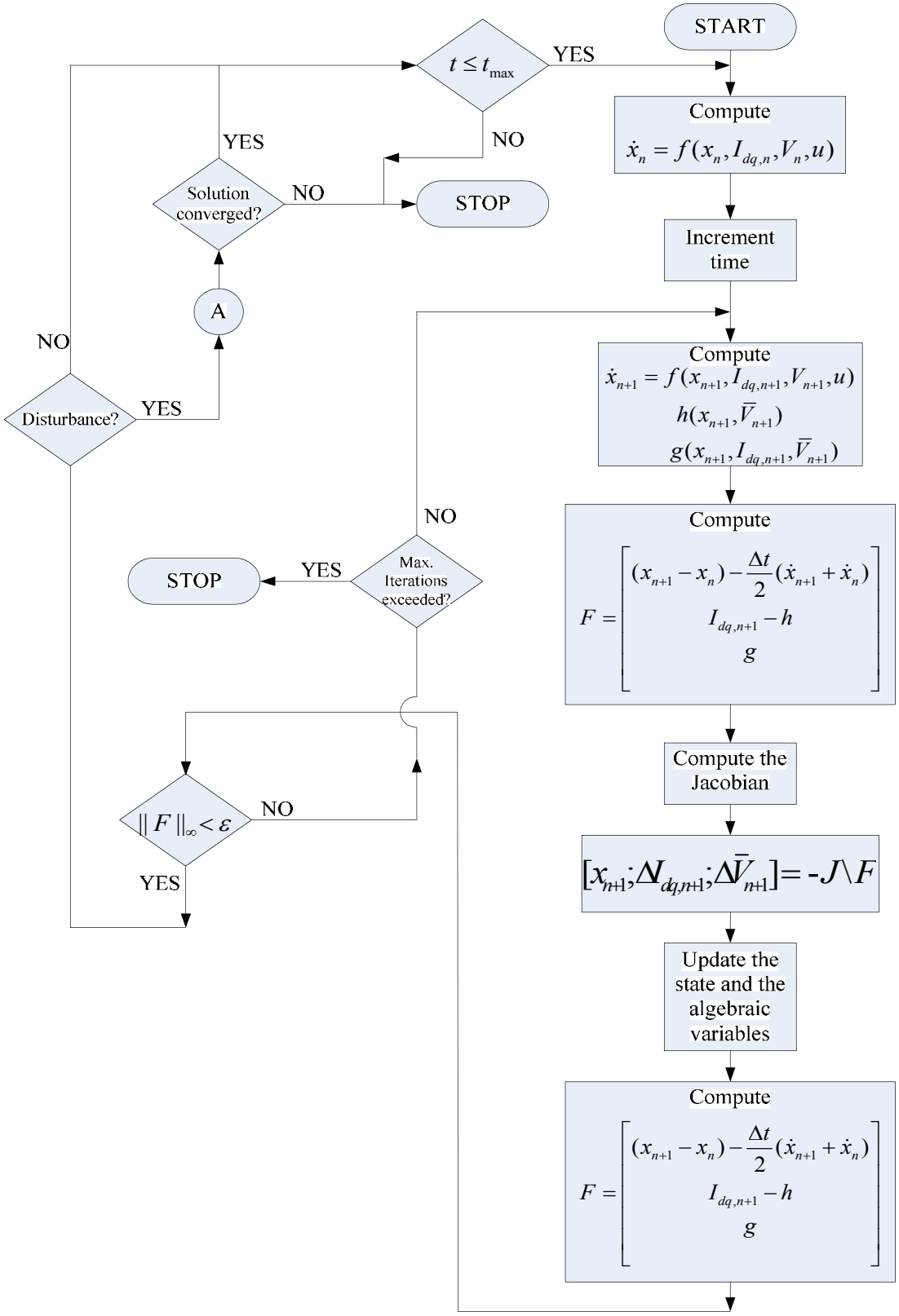

Figure 3.2 Transient stability simulation flowchart in power-balance Form

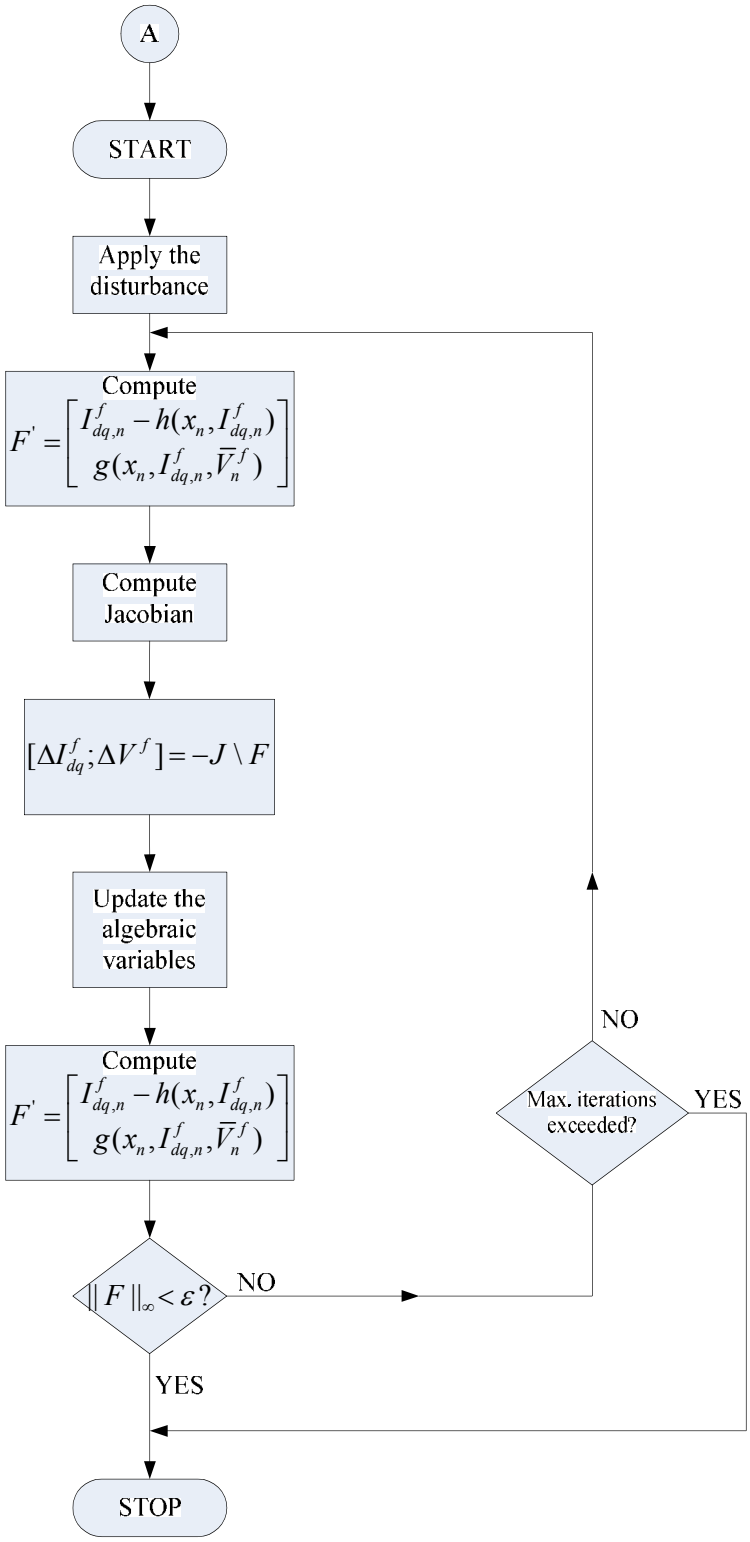

Figure 3.3 Disturbance solution

CHAPTER 4

INSTANTANEOUS TIME DOMAIN SIMULATION

The operation of a power system involves a continuous interaction of electromechanical and electromagnetic energy. During steady state, these energy exchanges are not modeled explicitly and the system behavior is represented by voltage and current phasors in frequency domain. Events such as switching or faults subject components to excessive current and voltage variations. Using a *quasi-steady* state approach, the electromagnetic energy exchanges are ignored and the electromechanical energy exchanges captured by modeling the network using phasor voltages and currents. However, when there is a large deviation in the frequency, the phasor representation becomes no longer valid. To obtain the energy exchanges thereafter, component modeling needs to be done at the electromagnetic transients level. Electromagnetic transients involve interaction between the magnetic field of inductances and electric field of capacitances in the system. These are very fast compared to the electromechanical transients which involve energy interactions between the mechanical energy stored in the rotating machines and the electrical energy stored in the network. This chapter describes the modeling of transmission lines and constant power loads for electromagnetic transients simulation.

4.1 Modeling of constant power loads

Constant power loads for steady state studies are modeled by fixed negative power injections into the network. There is no dependence of voltage on the constant power loads. Such modeling is based on the time period of interest involved in steady state studies.

Physically however, any device can be thought of as sensing the stimulus first before reacting to it. Thus, a load having constant power characteristics reacts to a change in the voltage or current after sensing it first. The quicker it responds, the more closer it is to absorbing constant power during the transient state. Our modeling of loads trying to absorb constant power is based on this notion.

Constant power loads are described by real and reactive power absorbed which is not an instantaneous term but rather the observation over one cycle of the fundamental frequency. Thus, the modeling requires observation of the instantaneous values over one cycle. The modeling of a constant power load for instantaneous time domain simulation is discussed below.

Consider a constant impedance load drawing complex nominal power $P_0 + jQ_0$ at a voltage magnitude V_0 across its terminals. The resistance and inductance of the load is given by

$$\begin{aligned} R &= V_0^{\,2} / P_0 \\ L &= V_0^{\,2} / \omega Q_0 \end{aligned} \tag{4.1}$$

here $\omega = 2\pi f$ and f is the fundamental frequency.

For a constant impedance load, if the voltage magnitude decreases, then the current drawn decreases and the load power decreases too since the load impedance is constant. For a load absorbing constant power however, if the voltage magnitude decreases, then the current increases to maintain constant power. This increase in the current as the voltage decreases can be modeled by decreasing the load impedance as the voltage decreases. Using equation 4.1, loads trying to absorb constant power are modeled by changing the resistance and the inductance of the load at each time step. This requires

the knowledge of the voltage magnitude V_0 at each time step. A *fourier* analysis of the voltage waveform over one cycle of the fundamental frequency gives the voltage magnitude at each time instant.

If n and n-1 represent the t_n and t_{n-1} time instants, the resistance and the inductance are modified at each time step as

$$\begin{aligned} R_n &= V_{n-1}^2 / P_0 \\ L_n &= (V_{n-1}^2 / \omega Q_0) \end{aligned} \tag{4.2}$$

here, the voltage magnitude V_{n-1} is calculated by performing a *fourier* analysis over a running window of one cycle of the fundamental frequency. The subscript $n-1$,associated with the voltage magnitude, indicates that the instantaneous voltages over one cycle of fundamental frequency ending at the $n-1$ time instant are used for the calculation of the voltage magnitude. Thus, the load responds to the voltage magnitude at the previous time instant.

4.2 Transmission line modeling

The section describes the modeling of single phase transmission lines. Two models are discussed here: Bergeron line model based on traveling wave theory and lumped parameter pi line models.

4.2.1 Bergeron model. Bergeron's model is an extension of the lossless transmission line model by incorporating the distributed series resistance of the line [13]. This type of model uses the traveling wave theory. The traveling wave theory is based on the phenomenon that energy is transferred along the line in the form of voltage and current

waves. Fig. (4.1) shows the propagation of current and voltage waves along a transmission line.

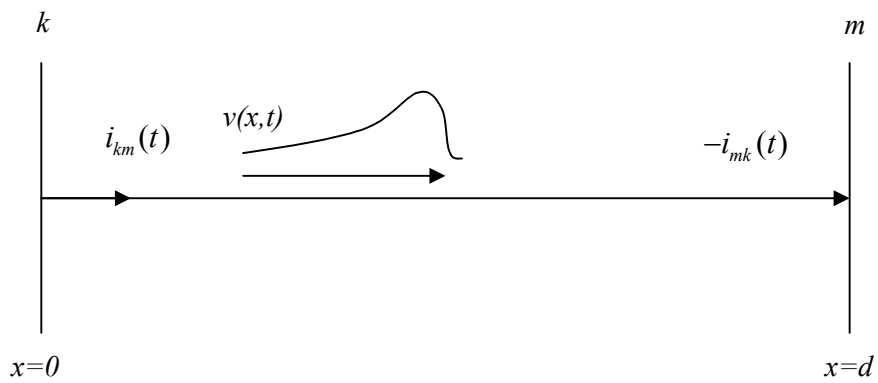

Figure 4.1 Propagation of a wave on a transmission line

ϖ is the velocity of the traveling wave and d is the length of the line. Assuming a lossless distributed parameter line with inductance L' and capacitance C' per unit length and solving the wave propagations equations, the transmission line model can be represented by a two-port network as shown in the Fig. 4.2

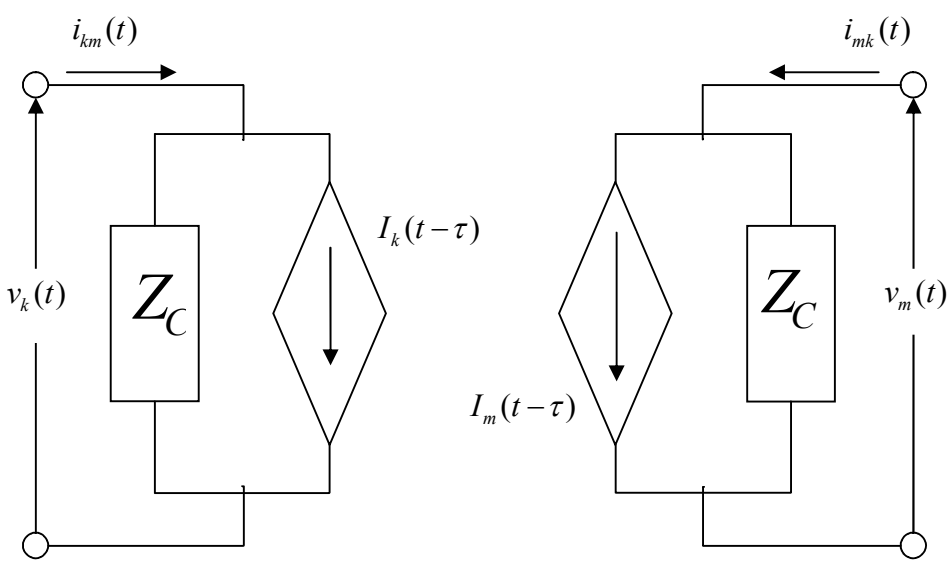

Figure 4.2 Equivalent two-port network for a lossless transmission line

$$Z_C = \sqrt{\frac{L'}{C'}}$$

$$\varpi = \frac{1}{\sqrt{L'C'}}$$

$$\tau = d / \varpi = d\sqrt{L'C'}$$

Z_C is the characteristic impedance of the line, ϖ is the wave velocity and τ is the time required for the wave to travel from one end to another. The current $i_{km}(t)$ is given as

$$i_{km}(t) = \frac{1}{Z_C} v_k(t) + I_k(t-\tau) \tag{4.3}$$

where, the current source $I_k(t-\tau)$ is

$$I_k(t-\tau) = -\frac{1}{Z_C} v_m(t-\tau) - i_{mk}(t-\tau) \tag{4.4}$$

Similar expression can be written for the current $i_{mk}(t)$,

$$i_{mk}(t) = \frac{1}{Z_C} v_m(t) + I_m(t-\tau) \tag{4.5}$$

where, the current source $I_m(t-\tau)$ is

$$I_m(t-\tau) = -\frac{1}{Z_C} v_k(t-\tau) - i_{km}(t-\tau) \tag{4.6}$$

As seen from the two port network given in Fig. 4.2, there is no direction connection between the line ends and the voltages and currents at one end are seen at the other end with a time delay equal to τ. Thus the line model does not have an instantaneous response like that assumed in the lumped parameter lines.

The Bergeron Model includes the series losses in the lossless line model by adding the distributed series resistance R' in lumped form. The total line resistance R is lumped one-fourth at the line ends and half at the middle of the line. This modeling is adequate enough and gives reasonable answers for $R/4 \ll Z_C$. The two port network for the Bergeron line model is shown in Fig. 4.3. The currents at both ends are given by the expressions

$$i_{km}(t) = \frac{1}{Z_C + \frac{R}{4}} v_k(t) + I'_k(t-\tau)$$

$$i_{mk}(t) = \frac{1}{Z_C + \frac{R}{4}} v_m(t) + I'_m(t-\tau)$$

The History term current source $I'_k(t-\tau)$ contains the voltages and the currents at both ends of the line and is given by

$$\begin{aligned} I'_k(t-\tau) = & \frac{-Z_C}{(Z_C + R/4)^2}(v_m(t-\tau) + (Z_C - R/4)i_{mk}(t-\tau)) \\ & + \frac{-R/4}{(Z_C + R/4)^2}(v_k(t-\tau) + (Z_C - R/4)i_{km}(t-\tau)) \end{aligned} \tag{4.7}$$

A similar expression can be written for the current source at the other end $I'_m(t-\tau)$.

$$\begin{aligned} I'_m(t-\tau) = & \frac{-Z_C}{(Z_C + R/4)^2}(v_k(t-\tau) + (Z_C - R/4)i_{km}(t-\tau)) \\ & + \frac{-R/4}{(Z_C + R/4)^2}(v_m(t-\tau) + (Z_C - R/4)i_{mk}(t-\tau)) \end{aligned} \tag{4.8}$$

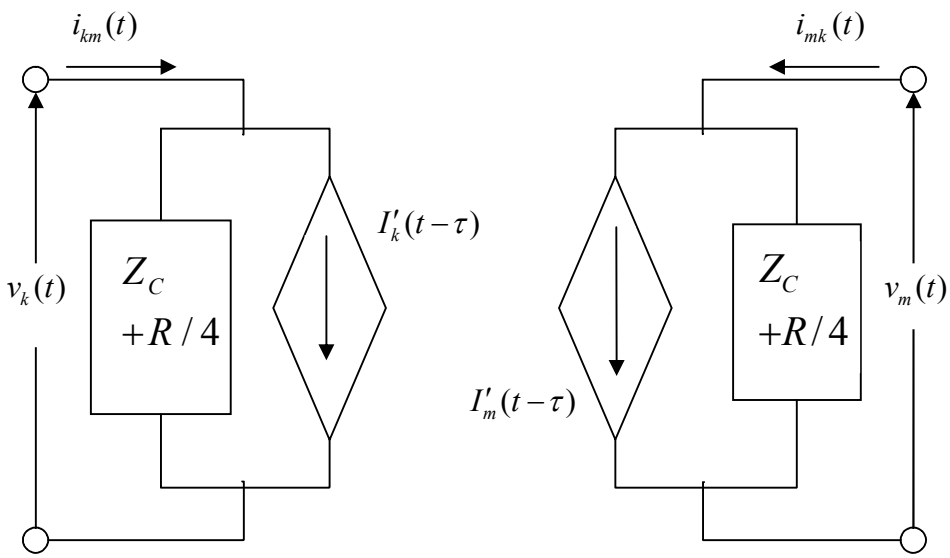

Figure 4.3 Bergeron transmission line model

4.2.2 Lumped model. A lumped model transmission line is modeled by lumping the distributed parameters. If, R', L' and C' are the distributed parameters of a line of length *d*, then the lumped parameters are obtained by multiplying the distributed parameters with the line length. The lumped parameter pi model is shown in Fig. (4.4). The relationship between the currents and the voltages at the two ends is obtained by using KCL and KVL at the two ends.

$$L\frac{di_{ser}}{dt} = v_k(t) - v_m(t) - Ri_{ser}(t) \tag{4.9}$$

$$\frac{C}{2}\frac{dv_k}{dt} = i_{km}(t) - i_{ser}(t) \tag{4.10}$$

$$\frac{C}{2}\frac{dv_m}{dt} = i_{ser}(t) + i_{mk}(t) \tag{4.11}$$

Where *R*, *L*, *C* are the lumped parameters of the line.

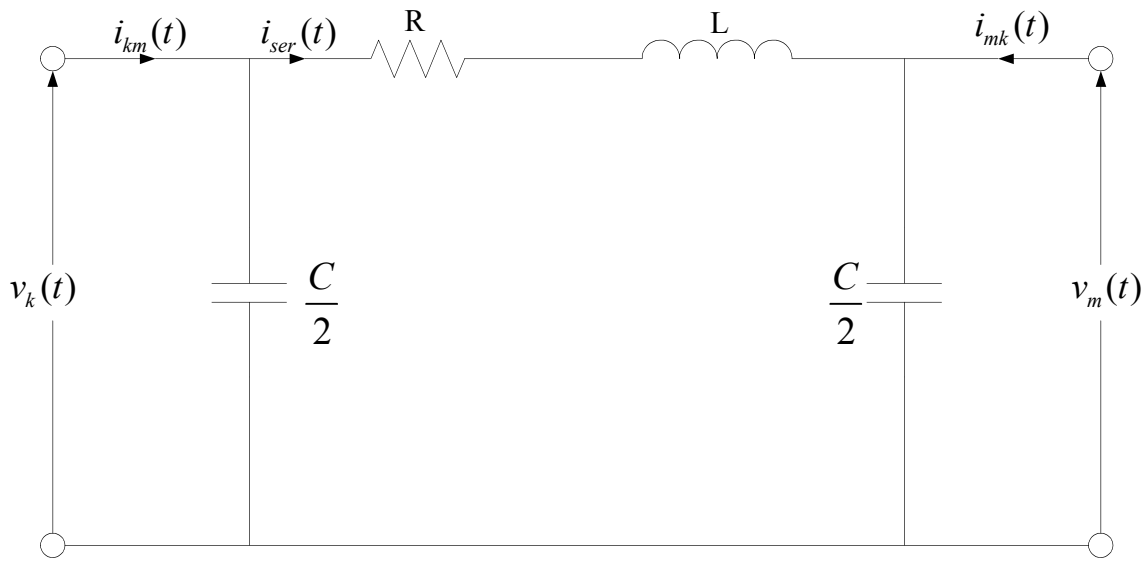

Figure 4.4 Lumped pi model of a transmission line

The formulation discussed in equations (4.9)-(4.11) can be extended to the modeling of three phase transmission lines. In matrix form, the system of equations for the three phase pi model transmission line can be written as

$$[L]\frac{di_{ser,abc}}{dt} = v_{k,abc}(t) - v_{m,abc}(t) - [R]i_{ser,abc}(t) \tag{4.12}$$

$$\frac{[C]}{2}\frac{dv_{k,abc}}{dt} = i_{km,abc}(t) - i_{ser,abc}(t) \tag{4.13}$$

$$\frac{[C]}{2}\frac{dv_{m.abc}}{dt} = i_{ser,abc}(t) + i_{mk,abc}(t) \tag{4.14}$$

where,

$$[R] \equiv \begin{bmatrix} R_{aa} & R_{ab} & R_{ac} \\ R_{ba} & R_{bb} & R_{bc} \\ R_{ca} & R_{cb} & R_{cc} \end{bmatrix}$$

$$[L] \equiv \begin{bmatrix} L_{aa} & L_{ab} & L_{ac} \\ L_{ba} & L_{bb} & L_{bc} \\ L_{ca} & L_{cb} & L_{cc} \end{bmatrix}$$

$$C \equiv \begin{bmatrix} C_{aa} & C_{ab} & C_{ac} \\ C_{ba} & C_{bb} & C_{cc} \\ C_{ca} & C_{cb} & C_{cc} \end{bmatrix}$$

If no coupling is present among the phases then the off-diagonal terms are zero. For balanced coupling, the [R], [L] and [C] matrices are symmetrical.

4.3 Generator modeling

The time span of interest decides the modeling of the generator used for studies. For the electromagnetic simulation, the fast acting dq axis fluxes and the damper windings fluxes are important to analyze the switching oscillations. On the other hand, for transient stability studies, which focus mainly on the speed variations, the subtransient reactances and the fast acting fluxes are neglected.

In this thesis, the generator model used for instantaneous time domain simulation is the same as that in Chapter 3. However, the interface between the network and generator has to be in terms of instantaneous voltages and currents. The interface is based on Park's transformation which involves conversion from phase to dq components and vice versa. The park's transformation matrices are

$$T_{dq} \triangleq \frac{2}{3}\begin{bmatrix} \sin(\theta) & \sin(\theta - 2\pi/3) & \sin(\theta + 2\pi/3) \\ \cos(\theta) & \cos(\theta - 2\pi/3) & \cos(\theta + 2\pi/3) \end{bmatrix}$$

$$T_{dq}^{-1} \triangleq \begin{bmatrix} \sin(\theta) & \cos(\theta) \\ \sin(\theta - 2\pi/3) & \cos(\theta - 2\pi/3) \\ \sin(\theta + 2\pi/3) & \cos(\theta + 2\pi/3) \end{bmatrix}$$

Note that in the above transformation, the zero sequence components are not considered as the generator is assumed star ungrounded. The interface between the

network and the synchronous machines using Park's transformation matrices is shown in Fig. (4.5).

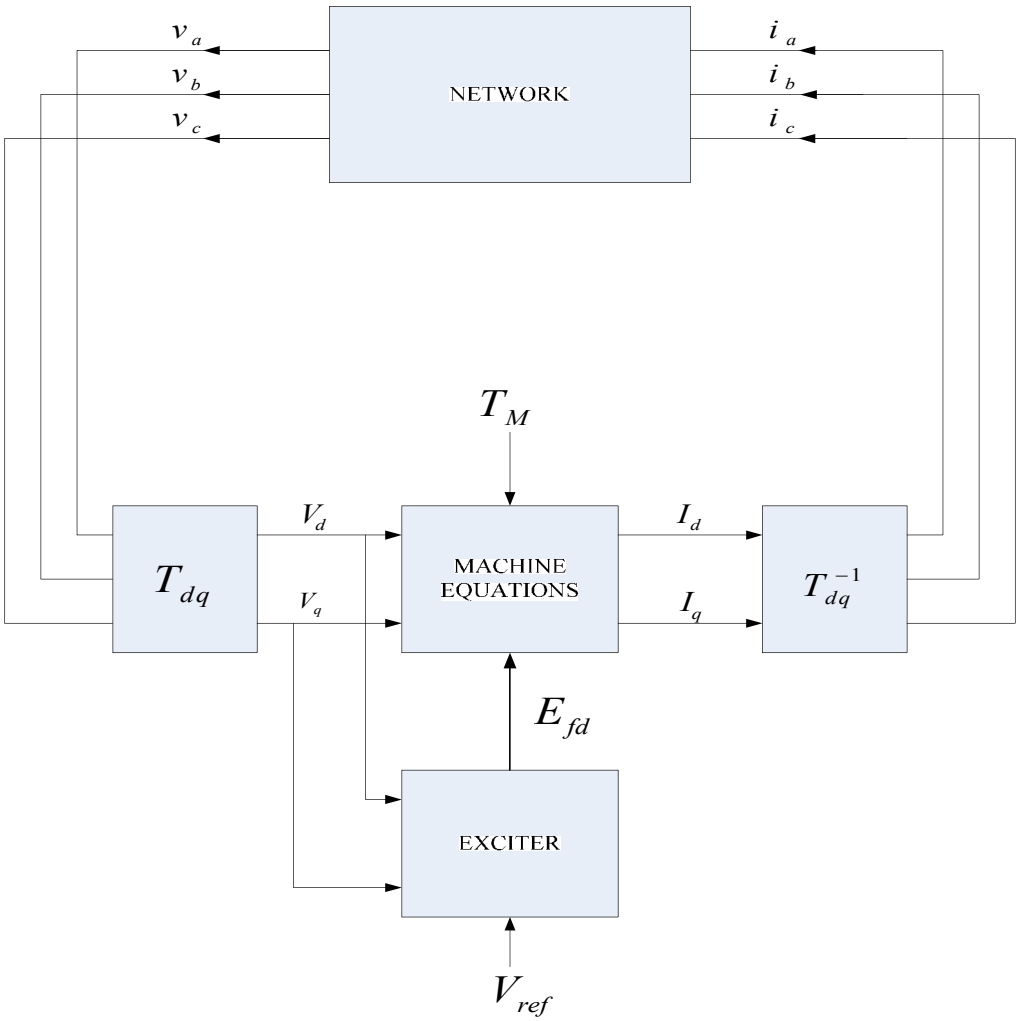

Figure 4.5 Machine-Network interface

4.4 Solution methodology

For single phase instantaneous time domain simulation or three phase simulation without the generator, the system of equations to be solved can be symbolically represented as

$$\begin{aligned} \dot{x}_{net} &= z(x_{net}, v, x_{load}) \\ \dot{x}_{load} &= d(x_{net}, v, x_{load}) \\ 0 &= g(x_{net}, v, x_{load}) \end{aligned} \tag{4.15}$$

where,

x_{net} are the network state variables namely the voltage across the capacitors and the current through the inductors.

v are the network voltages

x_{load} are the load state variables namely the current through load inductances assuming that the load has a lagging *pf*.

If the system includes a generator, then the system of equations can be represented as

$$\begin{aligned} \dot{x}_{gen} &= f(x_{gen}, I_{dq}, v) \\ I_{dq} &= h(x_{gen}, v) \\ \dot{x}_{net} &= z(x_{gen}, I_{dq}, v, x_{net}, x_{load}) \\ \dot{x}_{load} &= d(x_{gen}, I_{dq}, v, x_{net}, x_{load}) \\ 0 &= g(x_{gen,} I_{dq}, v, x_{net}, x_{load}) \end{aligned} \tag{4.16}$$

where,

x_{gen} are the generator and exciter state variables.

I_{dq} are the machine currents in the *dq* reference frame.

For the system defined given by equation 4.15, the interface between the generator and the network is done using the Parks' Transformation matrices. This interface is shown in Figure 4.5. The generator, exciter state variables and the *dq* axis currents are a part of the equation $\dot{x}_{load} = d(x_{gen}, I_{dq}, v, x_{net})$ only if the load is attached at the generator terminals. Equations 4.15 and 4.16 are solved for the state variables and the network voltages at each time instant using a numerical integrator like the trapezoidal integrator. In this thesis, MATLAB's Ode23t solver, which is a variable step size trapezoidal integrator, has been used to solve these equations because of its robustness.

CHAPTER 5

SIMULATION RESULTS AND DISCUSSION

For the simulations, Matlab based package MATPOWER ver. 2.0 and Simulink 6.0 based package Power System Blockset were used. MATPOWER is a package of Matlab M-files for solving power flow and optimal power flow problems developed by *Ray Zimmerman* and *Deqiang Gan* of PSERC at Cornell University. Some of the MATPOWER codes were used as support routines for the transient stability code. More information on MATPOWER can be found in [14]. Power System Blockset is a Simulink based package for analysis of electric power systems. It includes models for generators, motors, transformers, transmission lines, power electronic equipment etc. Instantaneous time domain simulation was done in Simulink using the Power System Blockset library blocks. The detailed information on Power System Blockset is given in [15].

The system data for the two bus system is given in Appendix A. The simulations done on the two bus system are discussed in the following sections. Throughout this chapter, the loading is described in terms of the real power P_d .However it should be noted that the load used in all the simulations has a power factor of 0.944.

5.1 Calculation of the steady state loading limit using continuation power flow

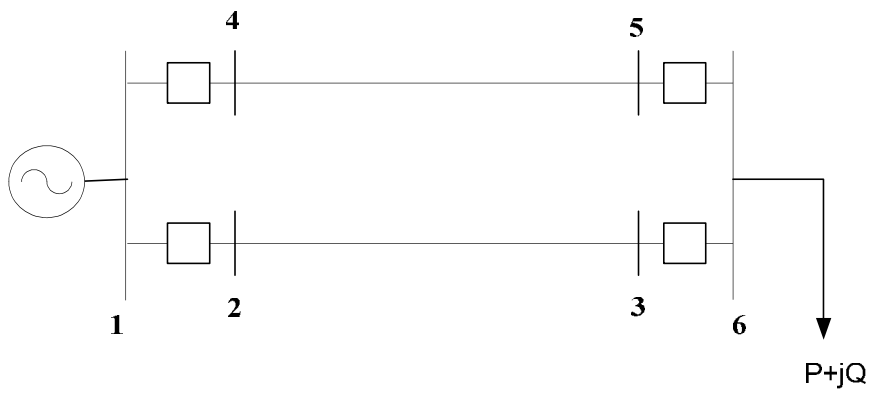

Figure 5.1 Test system topology

Figure 5.1 shows the one line diagram of the two bus test system used for continuation power flow. It consists of two transmission lines in parallel, Branches 2-3 and 4-5, with breakers at either ends. Breakers were inserted in the network by using fictitious buses 2,3,4,5. The load is a constant power factor PQ load and the generator is attached to a swing bus.

Prior to running the transient stability simulations, a continuation power flow was run to determine the steady state loadability of the system. Figure 5.2 shows the continuation power flow PV curves for the system with both lines in service and one line out. The steady state loading limit for the system with one line in service, $P^*_{d,ctgc}$, was found to be approximately 3.53 pu and with both lines in service, $P^*_{d,normal}$, was around 7.05. Note that the continuation power flow curves assume that the generator terminal voltage is maintained constant at 1.0 pu, however during the transient this is not true.

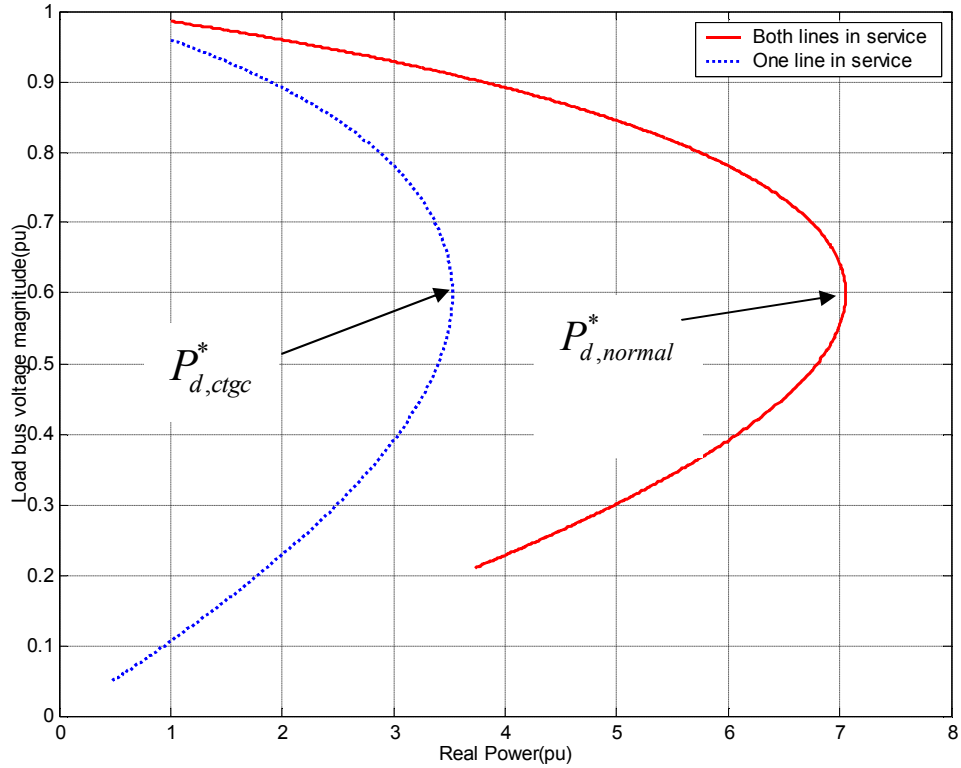

Figure 5.2 PV curves from continuation power flow

5.2 Transient stability simulations

For the solution of the DAE system, the network equations were written in the power balance form and the generator was modeled using the differential equations discussed in Chapter 3.

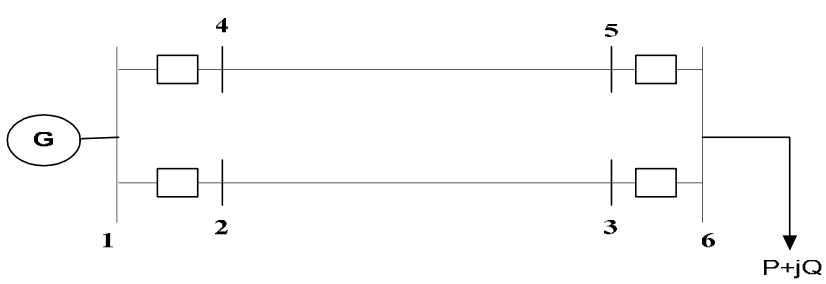

Figure 5.3 One line diagram of the two bus system for transient stability simulation

With the continuation power flow as the basis for the transient stability studies, the transient stability simulations were carried out by tripping branch 4-5 at 0.2 seconds. The basic aim of the transient stability simulations was to determine whether the system can survive the transient and reach the corresponding steady state operating point on the PV curve with one line in service. The line tripping was modeled by taking out branches 1-4, 4-5 and 5-6. The load was assumed to hold its constant PQ characteristic throughout the transient. The response of the system to line tripping at various loading levels is described in the following sections.

5.2.1 Loading upto 2.31 pu. The first simulation involved the transient analysis of the system for a loading level of P_d = 1.0 pu. The response of the system to tripping a line is shown in Figures 5.4 -5-5.

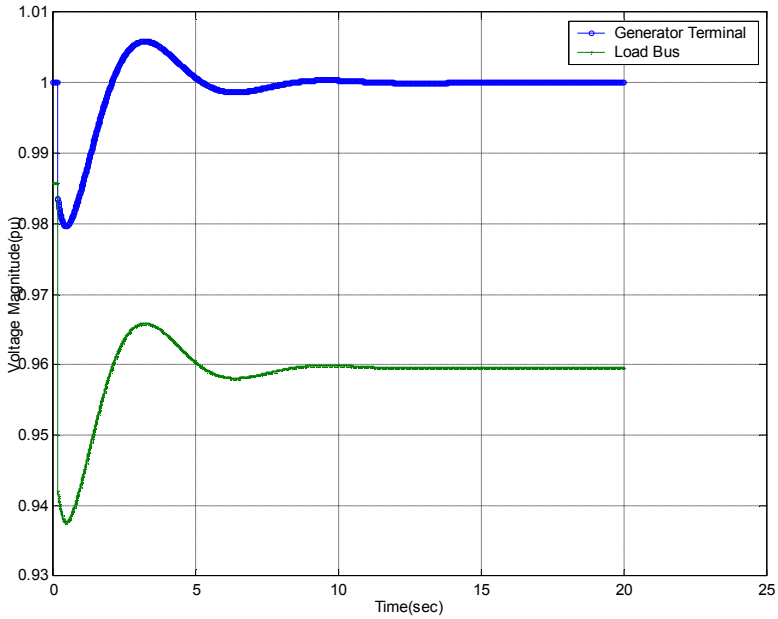

Figure 5.4 Voltage magnitude plot for line tripping at P_d = 1.0 pu

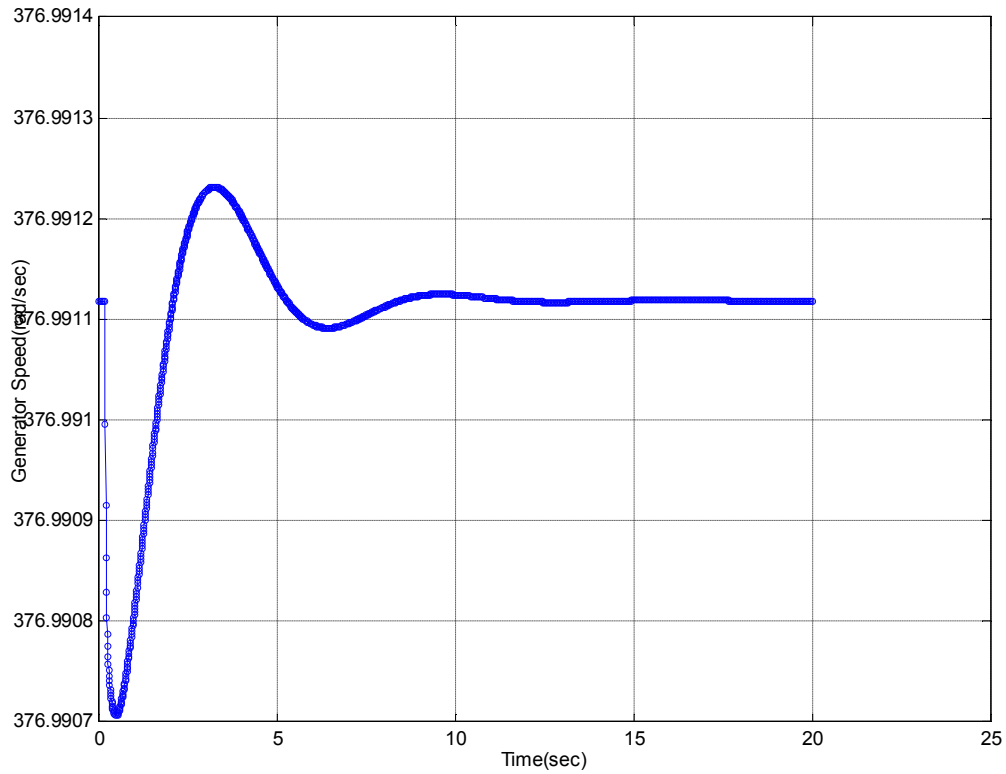

Figure 5.5 Generator speed plot for line tripping at P_d = 1.0 pu

Initially the system is operating at a point corresponding to P_d = 1.0 pu on the continuation power flow curve for both lines in service. When one line is taken out of service at 0.2 seconds, a one step solution of the algebraic equations is carried out to reflect the instantaneous change in the algebraic variables. At this time, a step change in the reference voltage to the exciter and the mechanical torque of the generator is done to reflect the control variables corresponding to the post-contingency operating point. Immediately after switching, there is a drop in the bus voltages. However the voltages recover and the system evolves through the transient and settles down at the operating point corresponding to P_d = 1.0 pu on the continuation power flow with one line in

service. The lowest dip in the load bus voltage is about 0.938 pu while at the generator terminals is about 0.98 pu.

Furthermore, it was seen that the system could survive through the transient to reach the post-contingency operating point for loading upto P_d = 2.31 pu. Figures 5.6-5.7 show the response of the system for P_d = 2.20 pu and 2.31 pu.

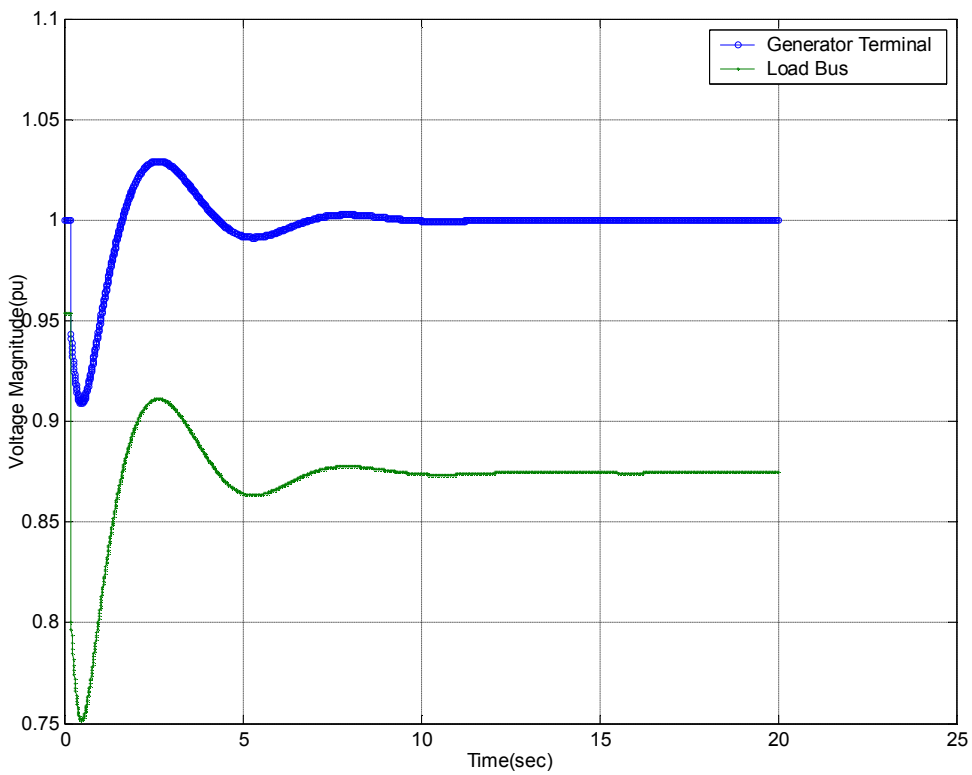

Figure 5.6 Voltage magnitude plots for line tripping at P_d = 2.20 pu

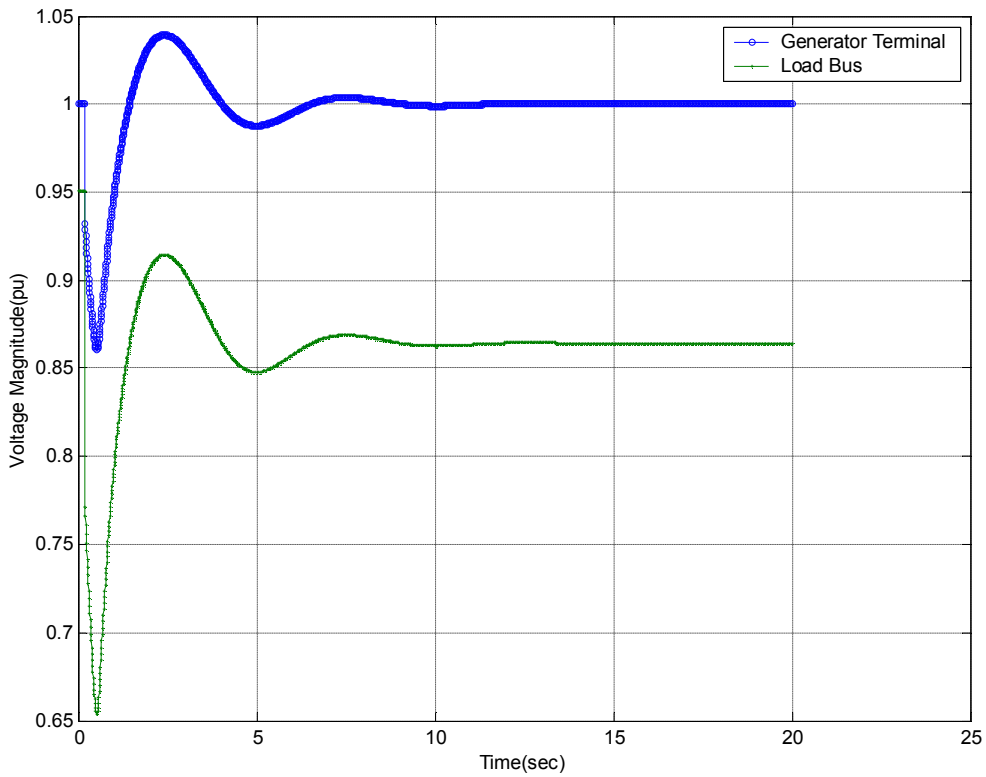

Figure 5.7 Voltage magnitude plots for line tripping at P_d = 2.31 pu

As seen from the plots, the drop in the bus voltage magnitudes, following the line switching, increases as the loading is increased. However, the system is able to survive the transient and settles down at the new operating point.

5.2.2 Loading at 2.32 pu. When the system load was increased to 2.32 pu, on switching, the DAE system was able to find the one step algebraic solution. But it could not find a solution at t = 0.428 seconds. Figures 5.8 and 5.9 show the voltage magnitude and the generator speed trajectories for this loading level.

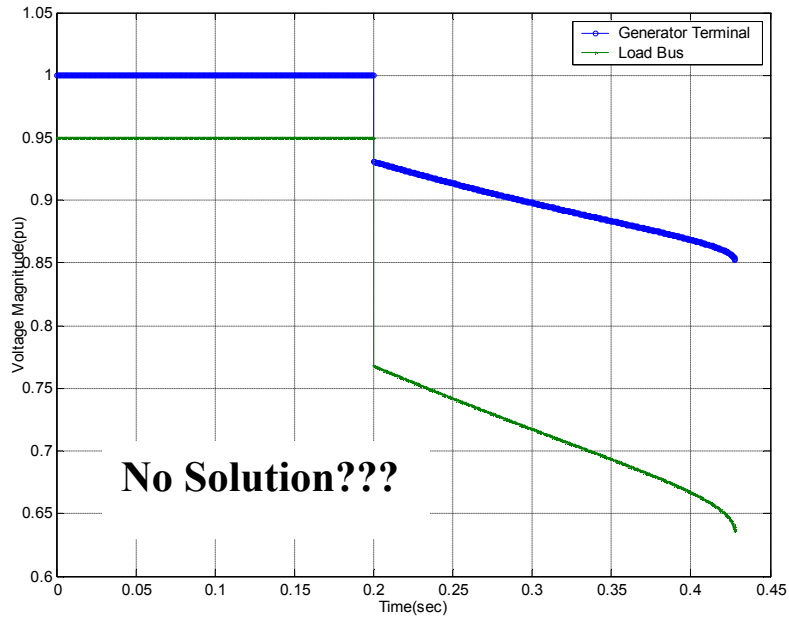

Figure 5.8 Voltage magnitude plot for line tripping at P_d = 2.32 pu

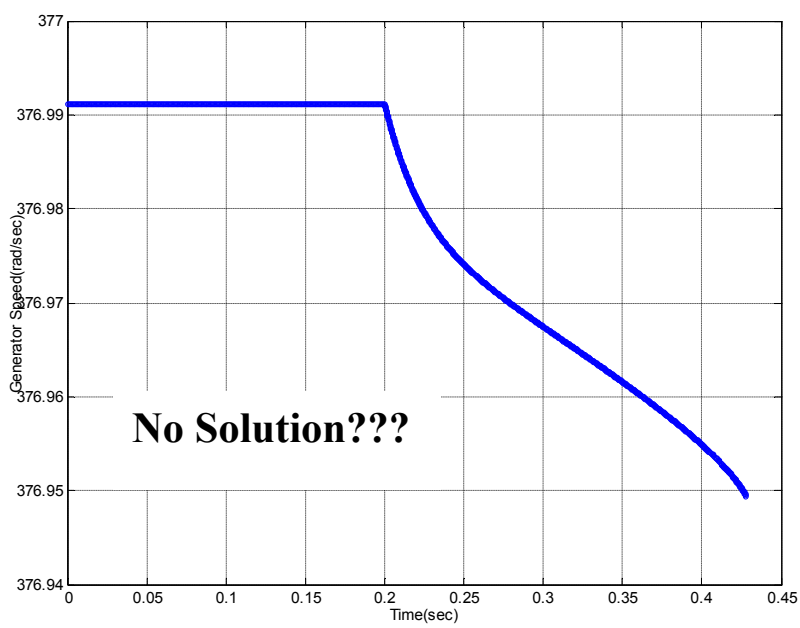

Figure 5.9 Generator speed plot for line tripping at P_d = 2.32 pu

Looking at Fig. 5.8, it can be seen that the load bus voltage magnitude has dropped below 0.65 pu. Intuitively, it can be perceived that the load bus voltage does collapse at the next step based on its slope and hence the system is not able to find the solution. However, the question arises then *Is the generator bus voltage collapsing too*? Seeing the generator bus voltage magnitude, this cannot be inferred. The continuing of the simulation was of paramount importance as only that could reveal the answer to why the solution is not converging and what the sequence of events following the non-convergence is.

5.2.3 DAE model assumptions validity. The DAE model is based on two major assumptions for network modeling. The first one is that the deviation in the frequency is small enough to allow the phasor representation. The second one is that all the nodes in the network respond instantaneously to the disturbance. We decided to check whether these assumptions are true beyond the non-convergence point. A distributed parameter line in which the network nodes respond to a disturbance with associated transmission line time delays was an alternative to test the instantaneous network response assumption. However, the distributed parameter lines required the solution process to be carried out using sinusoidal voltages and currents rather than phasors.

5.3 Instantaneous time domain simulation

In search of answer for the non-convergence of the DAE system, the instantaneous time domain simulations were run to match up the continuation power flow results. The continuation power flow or the power flow methods assume that the generator terminal voltage is fixed. Hence, for the instantaneous time domain simulation,

the source was represented by a constant voltage source. The test system used is shown in Figure 5.10.

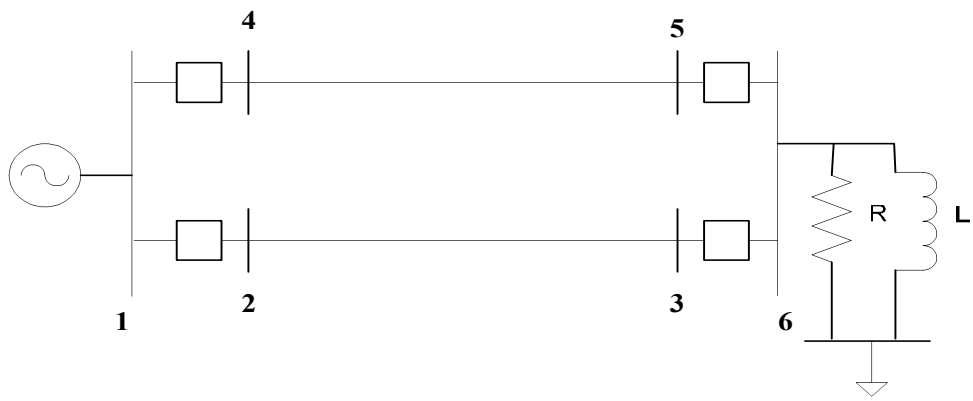

Figure 5.10 Test system for instantaneous time domain simulation

The transmission lines, Branches 4-5 and 2-3, were modeled as distributed parameter lines. Branches 1-2, 1-4, 3-6, 5-6 have breakers which are modeled by a series resistance. The load was modeled by a voltage dependent impedance load trying to draw constant power as discussed in Section 4.1. The data for the system used can be found in Appendix A. The loading was progressively increased with the load power factor fixed at 0.944. The response of the system to loading variations is described in the following sections.

5.3.1 P_d = 2.0 pu. Figure 5.11 shows the load bus voltage for branch 4-5 tripping scenario at this loading level. Branch 4-5 tripping was simulated by opening the breakers on branches 1-4 and 4-6. The tripping of the breakers was done at their respective current zero crossing. Following the branch tripping, the load power dips as the load is modeled as a voltage dependent impedance load based on the voltage magnitude seen at the previous time instant. However, the load recovers to draw the rated power eventually and

the system settles down at the new steady state value corresponding to the PV curve in Fig. 5.2 with one line in service and the loading at 2.0 pu.

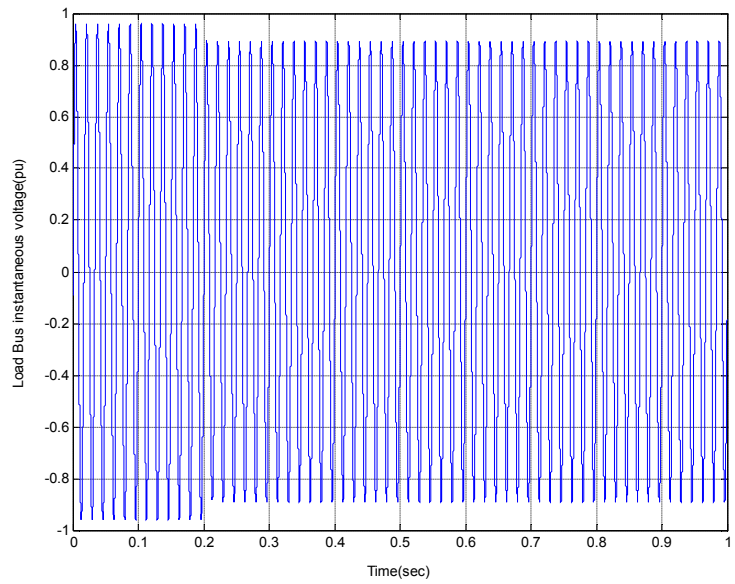

Figure 5.11 Load bus instantaneous voltage for branch 4-5 tripping at $P_d = 2.0$ pu

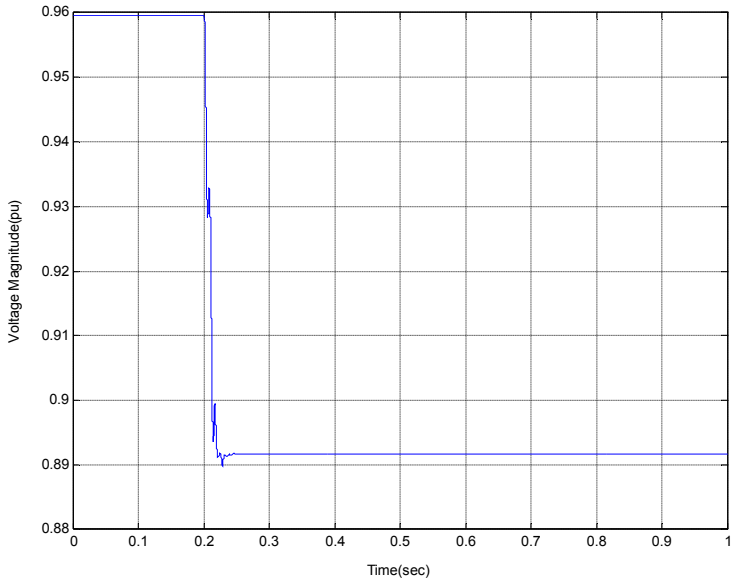

Figure 5.12 Load bus voltage magnitude for branch 4-5 tripping at $P_d = 2.0$ pu

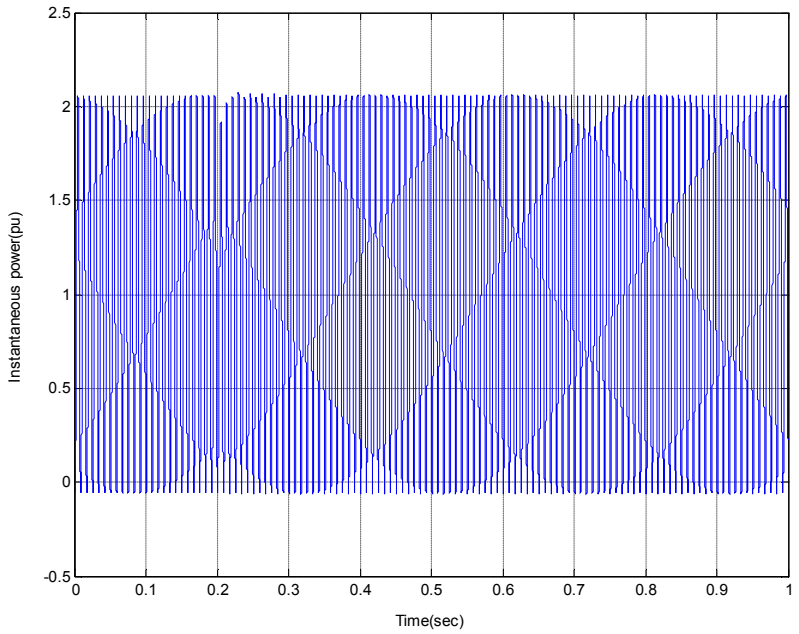

Figure 5.13 Instantaneous power drawn by the load.

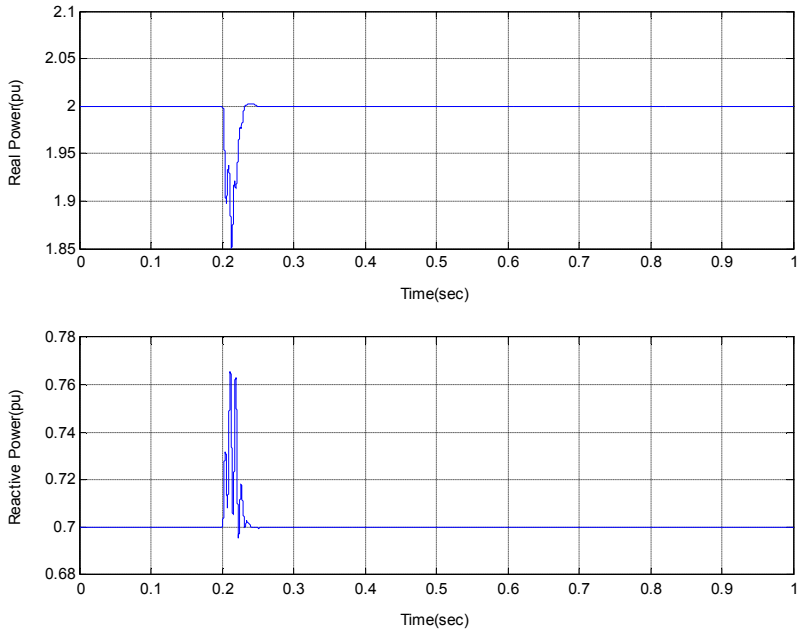

Figure 5.14 Real and reactive power drawn by the load

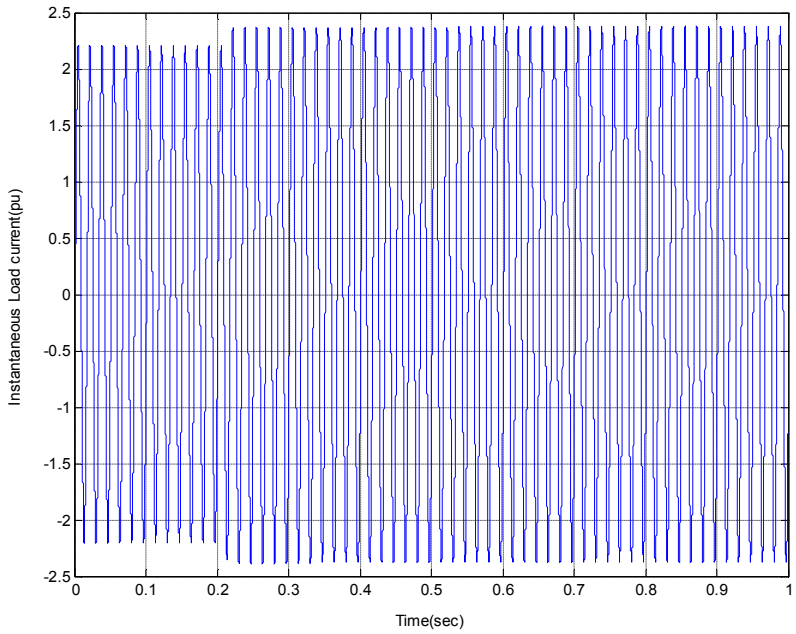

Figure 5.15 Instantaneous load current

5.3.2 P_d = 3.5 pu. The loading was then increased to P_d = 3.50 pu. This loading level is very close to the loading limit for the system with only one line in service ($P^*_{d,ctgc}$ = 3.53 pu). When a line was tripped at this loading level, the system survived the transient and settled down at a new steady state operating point. This operating point matches up with that shown in the continuation power flow curve with one line in service at a loading level of 3.50 pu. Figures 5.16-5.20 show the response of the system to line tripping at this loading level.

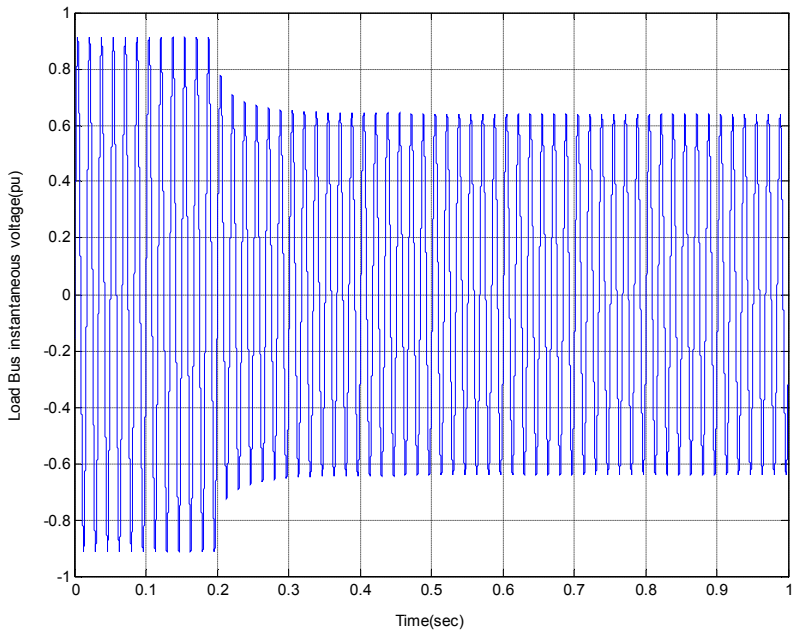

Figure 5.16 Load bus instantaneous voltage for branch 4-5 tripping at $P_d = 3.51$ pu

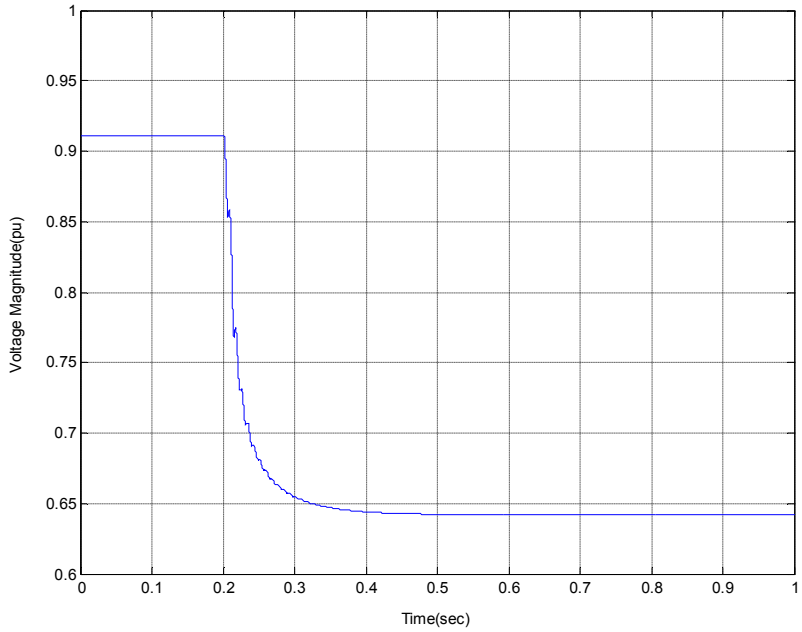

Figure 5.17 Load bus voltage magnitude

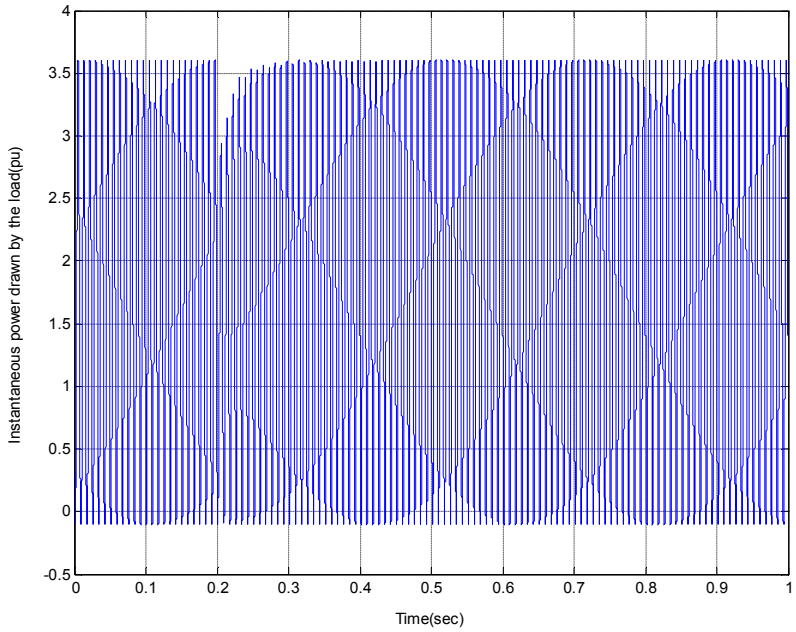

Figure 5.18 Instantaneous power drawn by the load

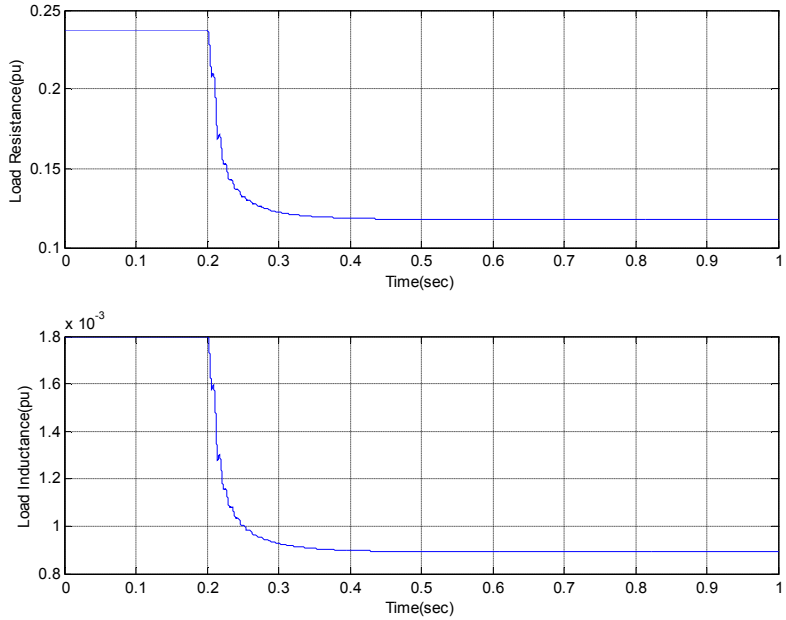

Figure 5.19 Load resistance and inductance

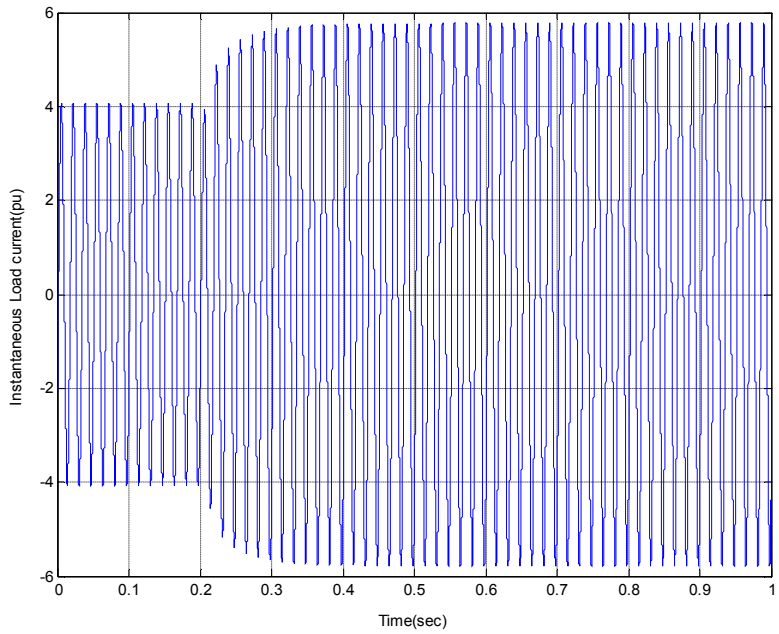

Figure 5.20 Instantaneous load current

Figure 5.19 shows the load resistance and inductance through the transient. As the voltage at the load bus drops, the resistance and the inductance reduce to draw more current. The load resistance and inductance settle down at a new steady state value as the voltage at the load bus settles down. This new value corresponds to the load impedance drawing P_d = 3.50 pu with one line in service.

5.3.3 P_d = 3.55 pu. The Real power loading level was now set to 3.55 pu which is beyond the post-contingency loading limit for the system ($P^*_{d,ctgc}$ = 3.53 pu).

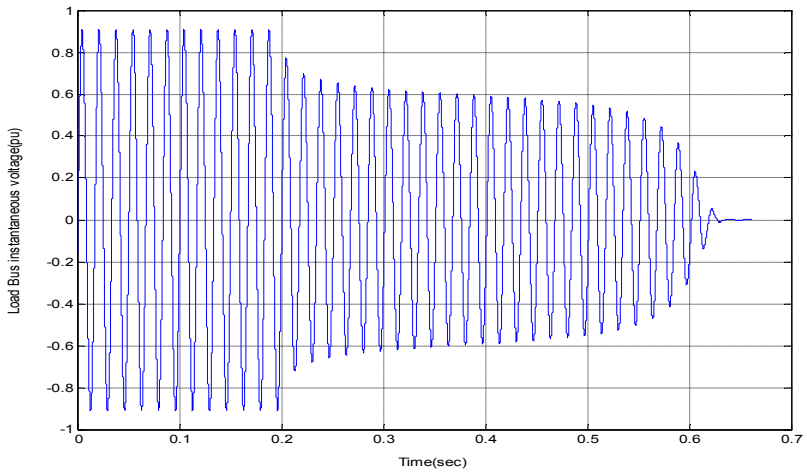

Figure 5.21 Load bus voltage collapse for branch 4-5 tripping at $P_d = 3.55$ pu

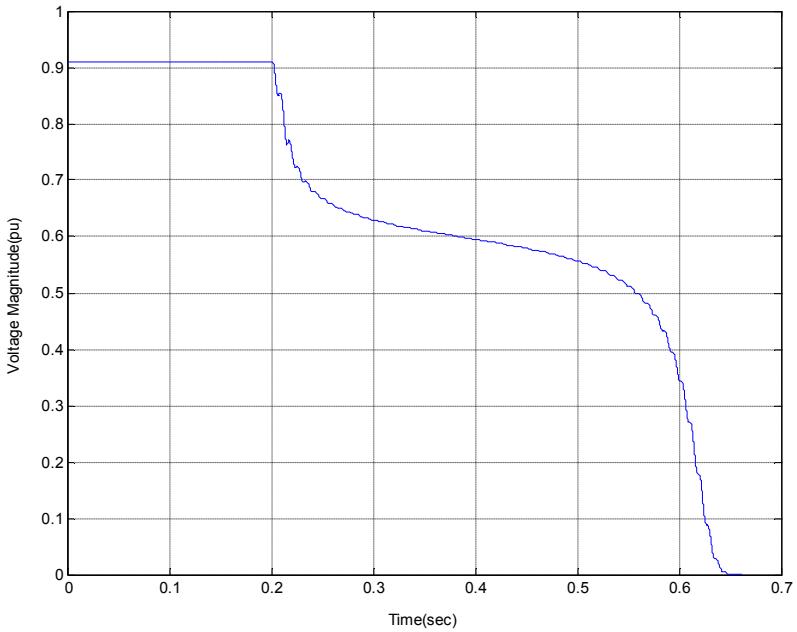

Figure 5.22 Load bus voltage magnitude

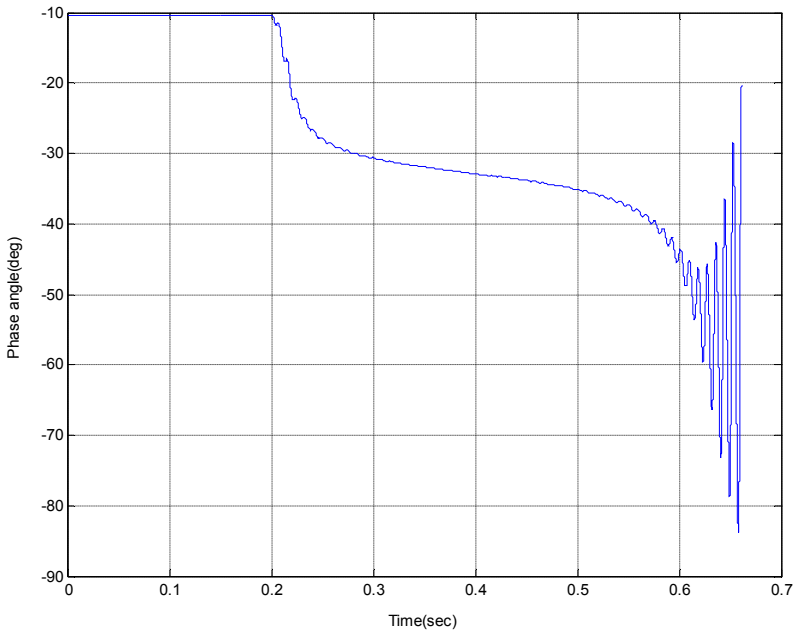

Figure 5.23 Load bus phase angle

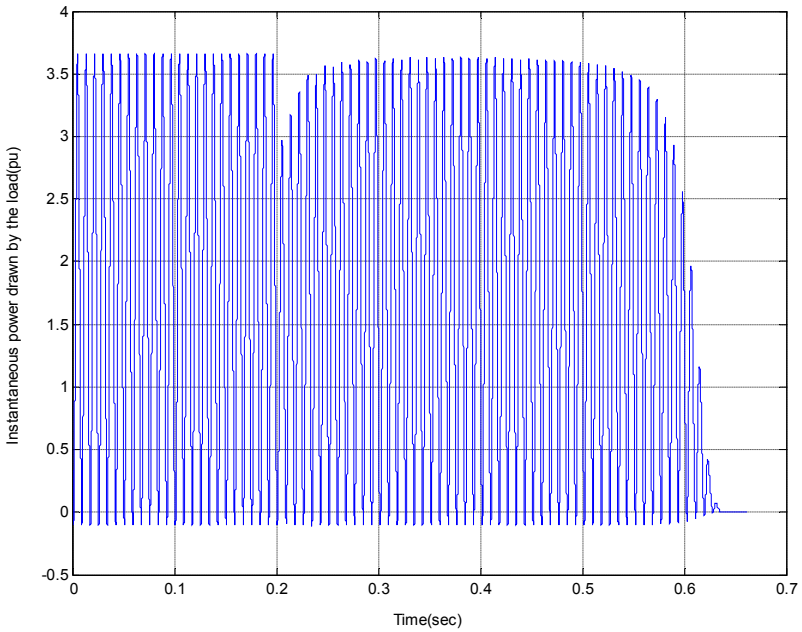

Figure 5.24 Instantaneous power

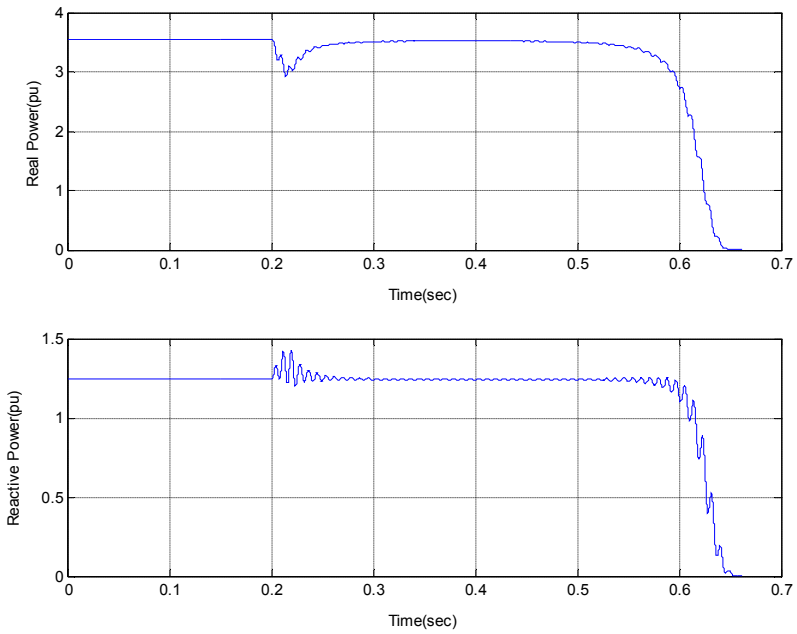

Figure 5.25 Real and reactive power

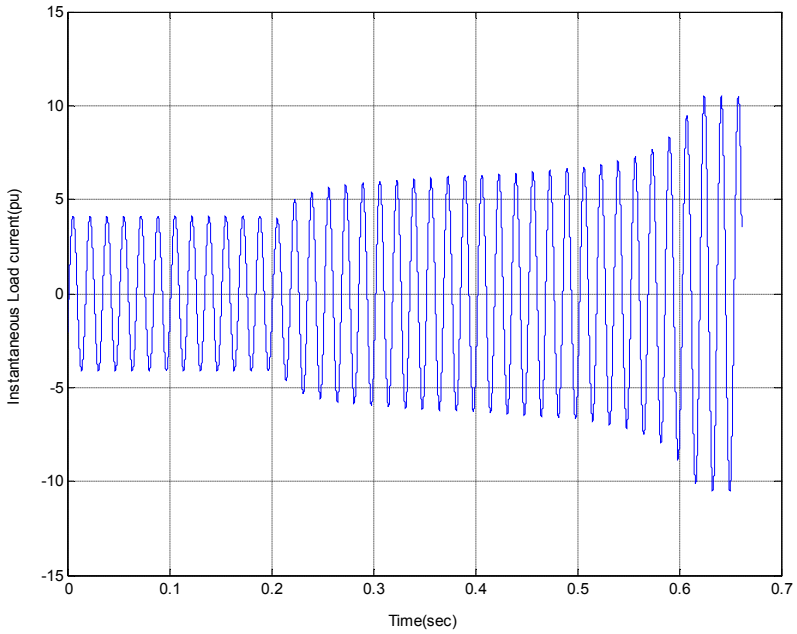

Figure 5.26 Instantaneous load current

As seen from the plots, at this loading level, there is no post-contingency operating point and the load bus voltage collapses. Due to the collapse in the voltage, the load cannot maintain its constant power characteristic and the instantaneous power drawn by the load drops to zero. The most interesting of the plots is the phase angle plot which shows an oscillation in the load bus phase angle as the voltage is collapsing. This suggests that the phasor assumption loses its validity at or beyond voltage collapse conditions. The instantaneous current, shown in Figure 5.26, settles down at a new value which is equal to the current drawn with the load shorted.

5.3.4 Voltage collapse capturing using lumped model. Use of a lumped parameter line instead of a distributed parameter line revealed that the voltage collapse can be captured using this model too. Figures 5.27-5.31 show the response of the system at the loading level of $P_d = 3.55$ pu using lumped parameter model.

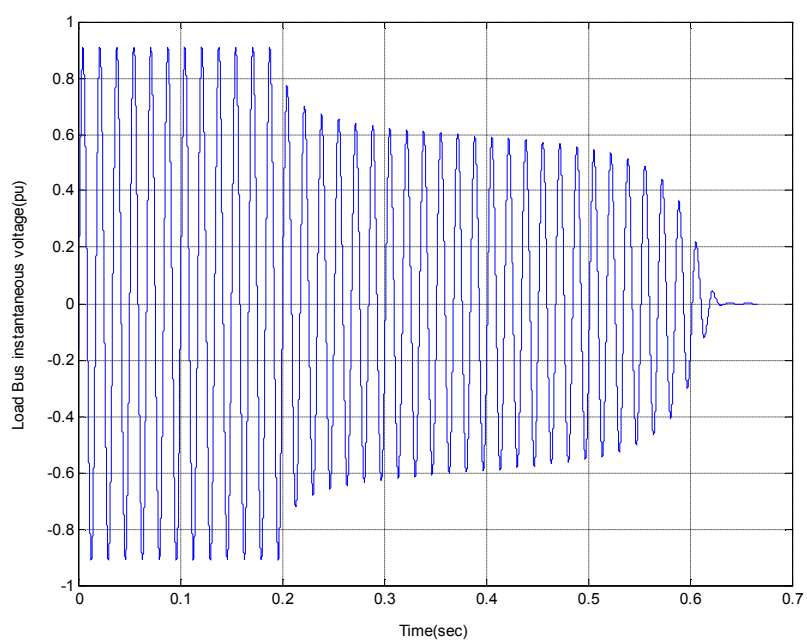

Figure 5.27 Load bus instantaneous voltage

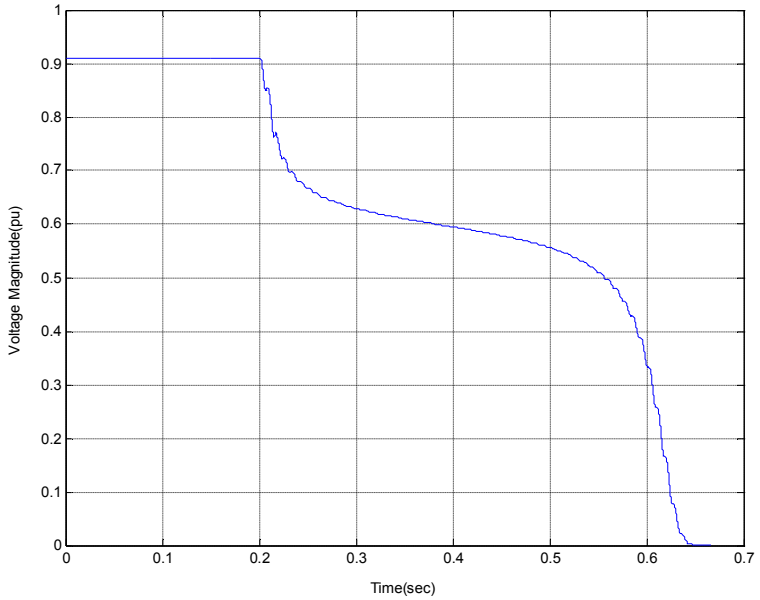

Figure 5.28 Load bus voltage magnitude

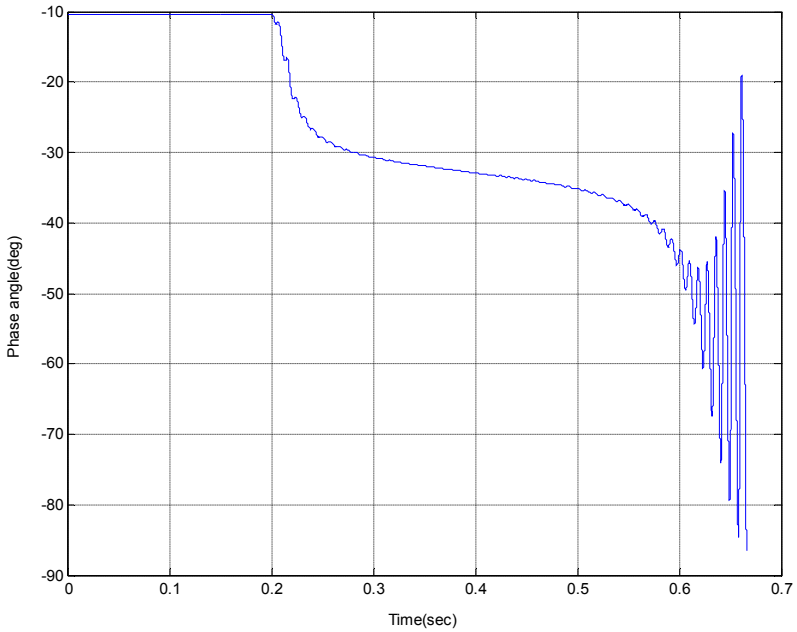

Figure 5.29 Load bus phase angle

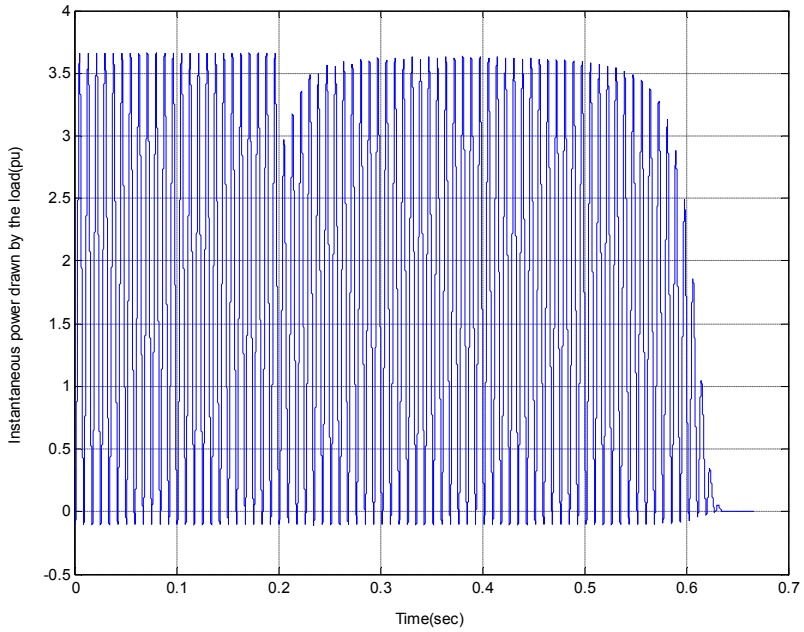

Figure 5.30 Instantaneous power

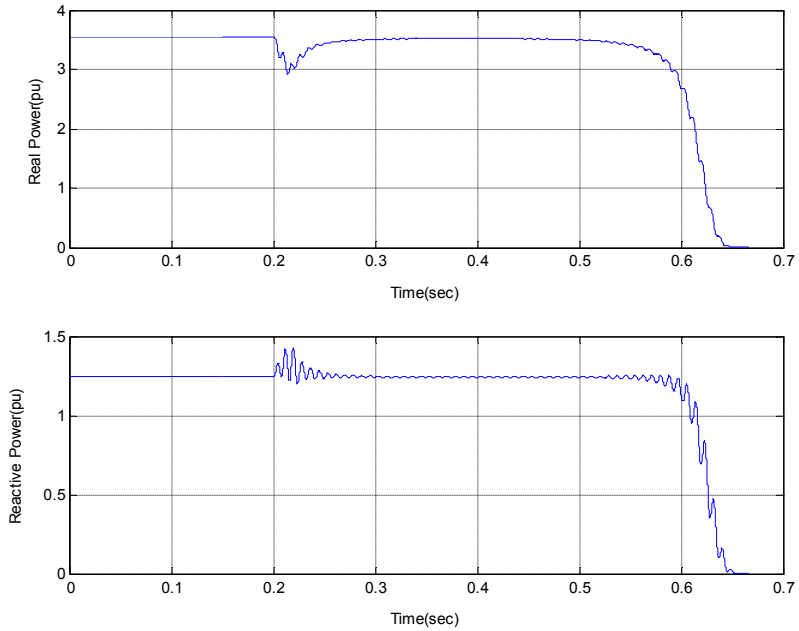

Figure 5.31 Real and reactive power

5.4 Two bus system with a generator model in instantaneous time domain

The source used for single phase instantaneous time domain simulation was a constant voltage source which is not a realistic source model. Three phase synchronous generators supply power in an electrical network and not constant voltage sources. Hence, the next step in the series of simulations involved setting up the two bus system in Instantaneous Time Domain Simulation with the generator included. For this purpose, modeling of the generator in SIMULINK required the three phase modeling of the system. The generator was modeled using the differential equations discussed in Chapter 3 and the generator-network interface discussed in Chapter 4. A three phase pi model from the Power System Blockset was used to model transmission lines on Branches 2-3 and 4-5. Three phase breaker models were used for the breakers on branches 1-2, 1-4, 3-6 and 5-6. The tripping of Branch 4-5 was modeled by opening the breakers on Branch 5-6 first followed by the opening of the breakers on Branch 1-4. The load was modeled as a balanced three phase star connected voltage dependent impedance load. To keep the load balanced at all times, the resistances and the inductances were updated based on the positive sequence voltage magnitude at the load bus as:

$$R_{abc,n} = \frac{V_{pos,n-1}^2}{P_0}$$

$$L_{abc,n} = \frac{V_{pos,n-1}^2}{\omega Q_0}$$

where,

n and *n-1* are the time instants t_n and t_{n-1}

R_{abc} is the load resistance and L_{abc} is the load inductance

V_{pos} is the positive sequence voltage magnitude at the load bus

P_0, Q_0 are the nominal real and reactive powers

The subscript $n-1$ used with the positive sequence voltage magnitude denotes that the calculation of V_{pos} is based on the instantaneous three phase voltages over one cycle of fundamental frequency ending at t_{n-1}.

The initialization of this system was done using a power flow solution followed by an initialization of the generator variables. The loading for the system was set at $P_d =$ 2.32 pu with a load *pf* of 0.9444, the loading at which a transient voltage collapse occurs. On observing the positive sequence load bus voltage magnitudes, the voltage magnitude seemed to recover instead of collapsing for this loading level. When the response of the real and reactive load power was seen, it was found that the load was reacting much slowly or with a larger delay to the change in the voltages.

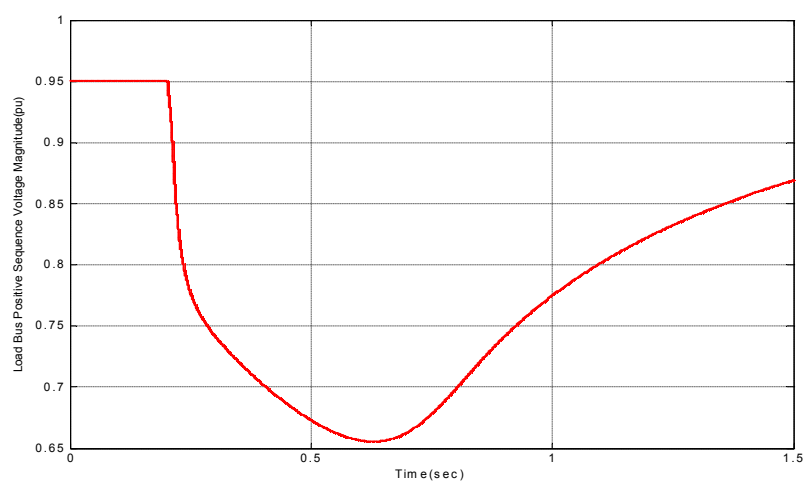

Figure 5.32 Positive sequence load bus voltage magnitude recovering for a loading $P_d = 2.32$ pu

When the response of the real and reactive load power was seen, it was found that the load was reacting much slowly or with a larger delay to the change in the voltages.

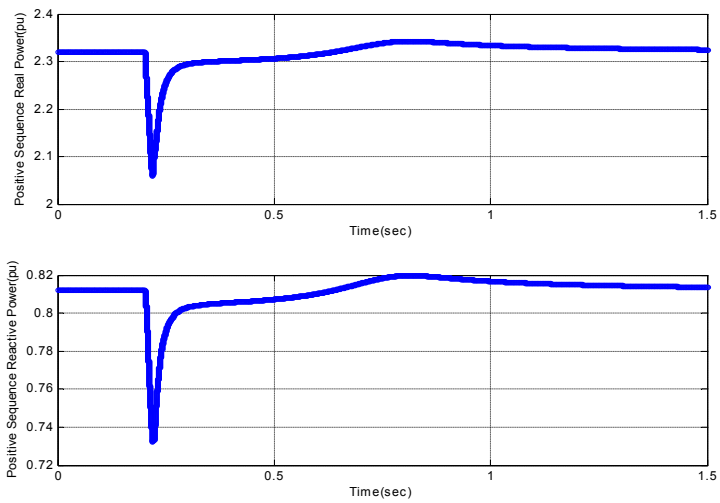

Figure 5.33 Positive sequence real and reactive power. $P_d = 2.32$ pu

On increasing the load to $P_d = 2.35$ pu, it was seen that the tripping of branch 4-5 at this loading level, causes a voltage collapse at the load bus. The collapse plots are shown in figures 5.34-5.35.

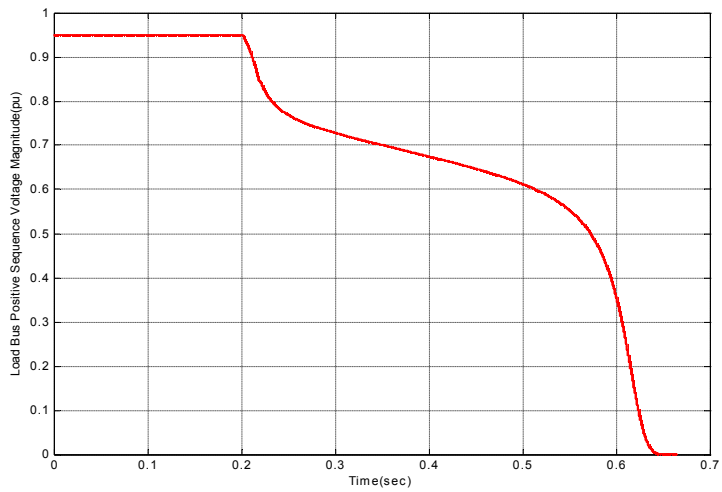

Figure 5.34 Positive sequence load bus voltage Magnitude. $P_d = 2.35$ pu

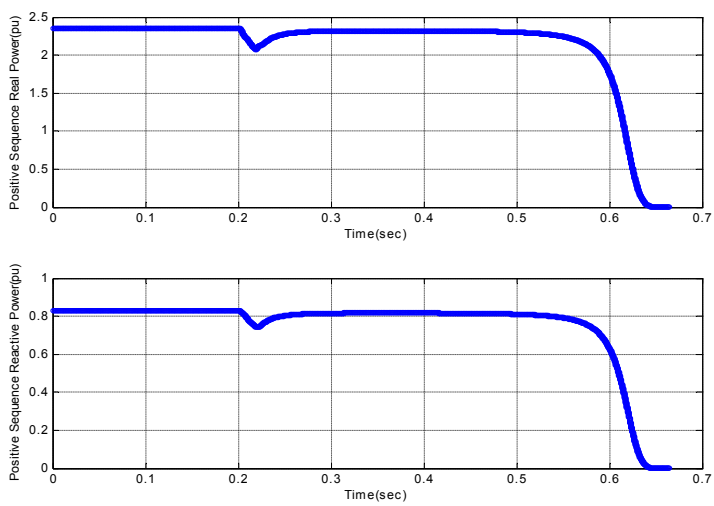

Figure 5.35 Positive sequence real and reactive power. $P_d = 2.35$ pu

5.5 Capturing voltage collapse using voltage dependent impedance load in transient stability simulations

The instantaneous time domain simulation results showed that the voltage collapse can be captured. The simulation results concurred with the continuation power

flow results. Beyond the steady state loading limit with one line in service, the load bus voltage collapses. The phasor assumption does not hold true at and beyond the collapse voltage level. Constant power load was modeled as a voltage dependent impedance load in instantaneous time domain simulation. Using this load model, it was found that the voltage collapse could be captured. This load model was then implemented back in the Transient Stability Simulation to investigate whether such a load model could capture the voltage collapse trajectories.

The modeling of a constant power load modeled as a voltage dependent impedance load for Transient Stability simulations is discussed in the following paragraphs.

If n represents the time instant t_n then a static impedance load is modeled in transient stability simulations as

$$\begin{aligned} P_n &= k_p V_n^2 \\ Q_n &= k_q V_n^2 \end{aligned} \tag{5.1}$$

where,

$$\begin{aligned} k_p &\equiv \frac{P_0}{V_0^2} \\ k_q &\equiv \frac{Q_0}{V_0^2} \end{aligned}$$

P_n is the real power drawn by the load at the nth time instant.

Q_n is the reactive power drawn by the load at the nth time instant.

P_0 is the nominal load real power.

Q_0 is the nominal reactive power.

V_0 is the nominal voltage magnitude

k_p, k_q are the load conductance and susceptance respectively which remain fixed for a constant impedance load. For a voltage dependent impedance load trying to draw constant power, these parameters have to increase as the voltage decreases. Using the concept of the load responding after it sees a change in the voltage; k_p, k_q values were modified at each time instant as

$$k_{p,n} \equiv \frac{P_0}{V_{n-delay}^2}$$
$$k_{q,n} \equiv \frac{Q_0}{V_{n-delay}^2} \tag{5.2}$$

where, $n-1$ is the time instant t_{n-1}, V_{n-1} is the voltage magnitude at t_{n-1}, and *delay* is the time required for the load impedance to change for a change in the load bus voltage.

To match up the delay in the load power recovery in the three phase instantaneous time domain simulation, transient stability simulation at this loading level was done by varying the delay. It was found that a delay of half a cycle or 0.8333 seconds closely matched with the results from the instantaneous time domain simulation. This delay found is related to the load time constant and has to be investigated in the future. The comparison of the transient stability simulation and instantaneous time domain simulations is shown in Figure 5.36 and 5-37.

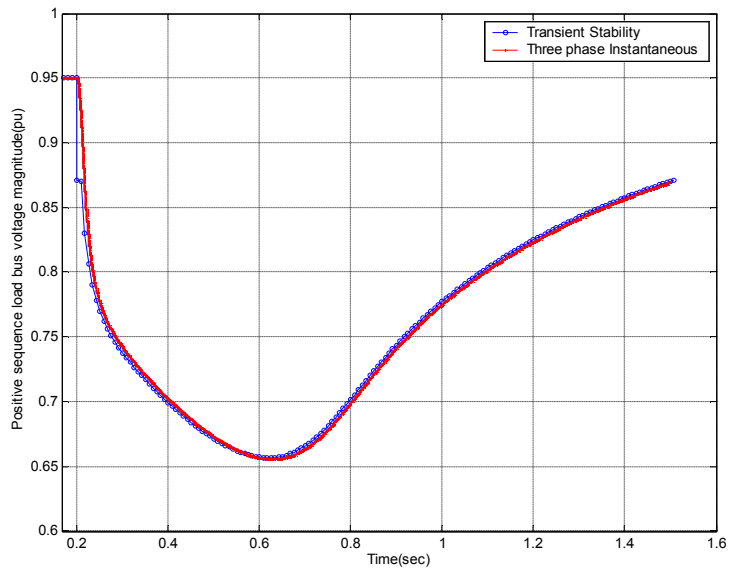

Figure 5.36 Positive sequence load Bus voltage magnitude. $P_d = 2.32$ pu

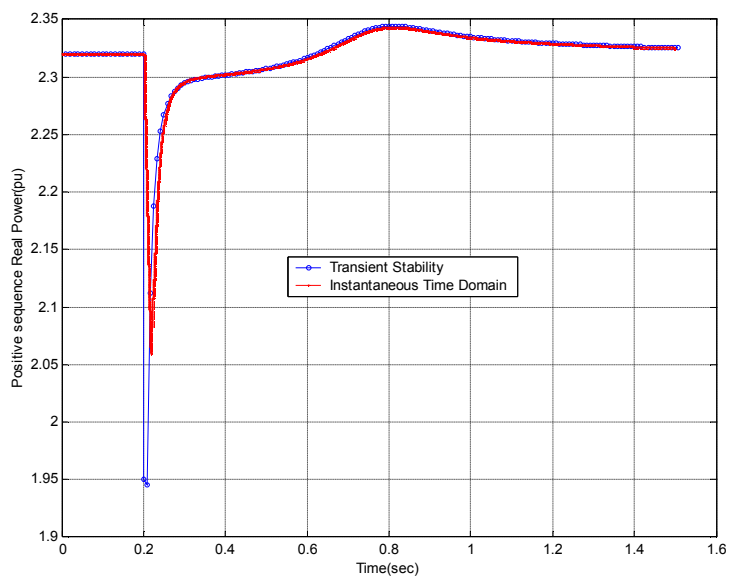

Figure 5.37 Positive sequence real power. $P_d = 2.32$ pu

The large difference in the real power just after the switching instant as shown in Figure 5.37 is due to the difference in the modeling of the load in the two simulations.

While the load is modeled as constant impedance at switching in the transient stability simulation, the load is modeled as a positive sequence voltage magnitude dependent load in the instantaneous time domain simulation.

The loading was then increased to $P_d = 2.35$ pu to see whether the system can handle this load. The response of the system from Transient Stability Simulation and Instantaneous Time Domain Simulation is shown in figures 5.38-5.39.

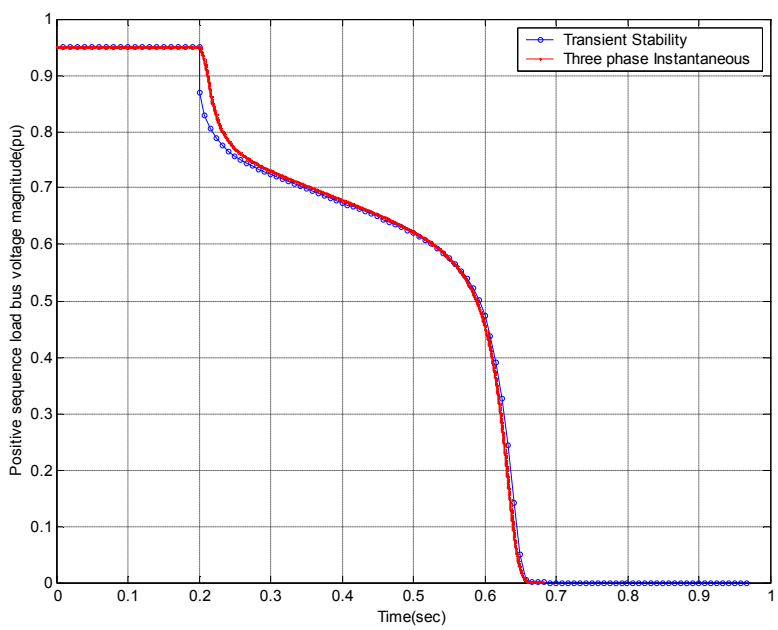

Figure 5.38 Voltage collapse at the load bus for line tripping at $P_d = 2.35$ pu

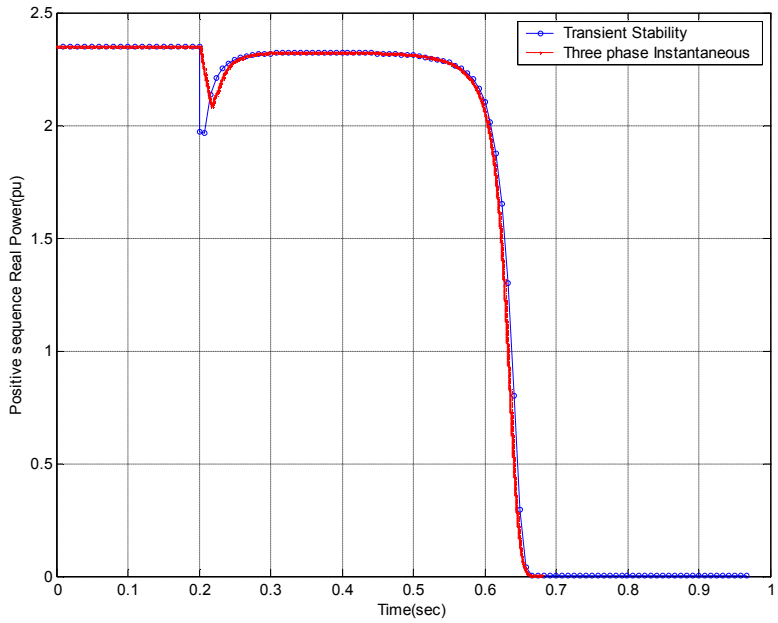

Figure 5.39 The load cannot recover as the voltage collapses at the load Bus.

As seen from figures 5.38-5.39, the load bus voltage collapses for branch 4-5 switching at a loading level of $P_d = 2.35$ pu.

For capturing the voltage collapse trajectories for loads which maintain constant power throughout the transient, the load delay was reduced to 0.1 millisecond so that the voltage dependent impedance load follows the constant power characteristic closely. The response of the system at a loading level of $P_d = 2.32$ pu is shown in Figures 5.40-5.42

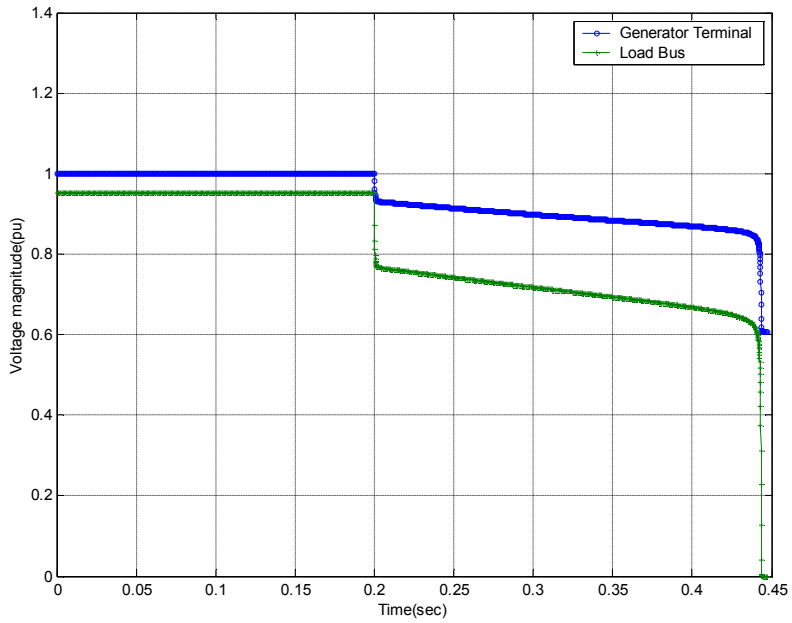

Figure 5.40 Collapse of load bus voltage captured in transient stability simulations using voltage dependent impedance load model.

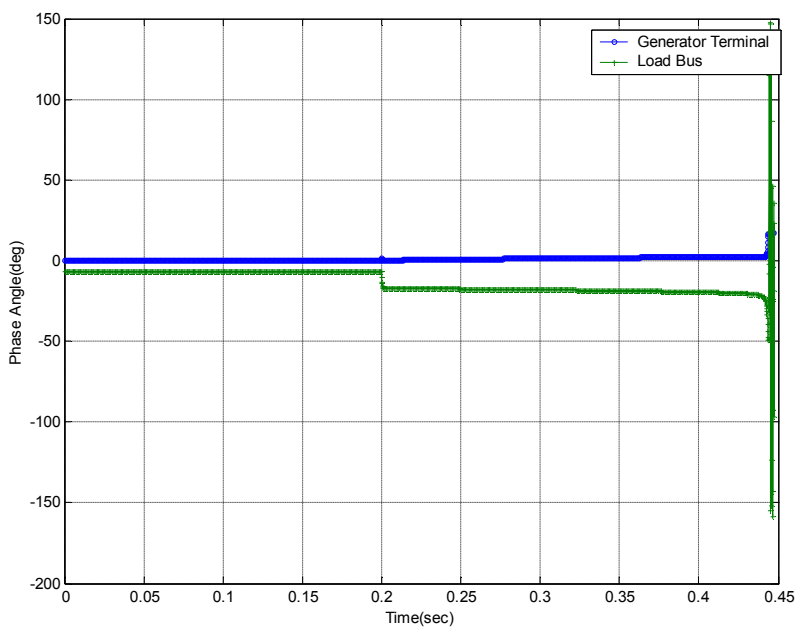

Figure 5.41 Phase angle oscillations at the load bus

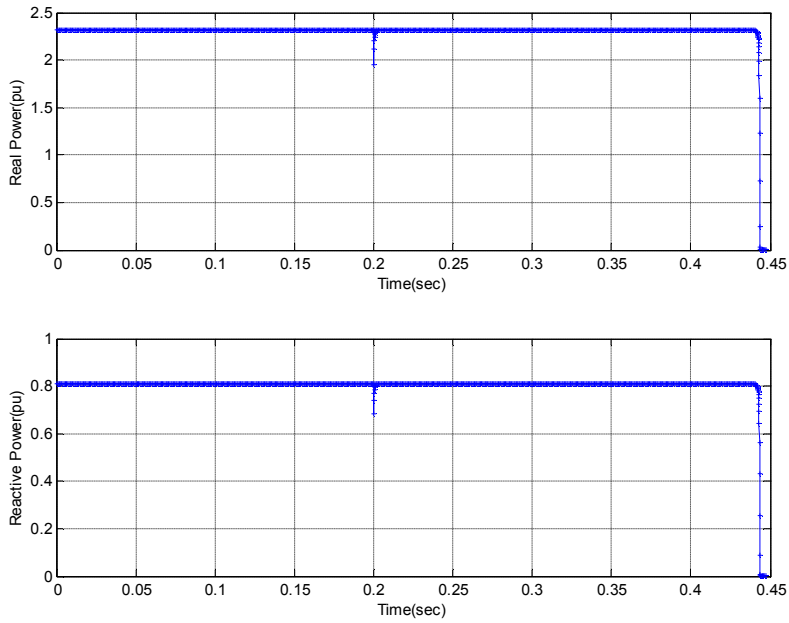

Figure 5.42 Power drawn by the load

As seen from Figures 5.40-5.42, the voltage collapse is captured in transient stability simulations using a voltage dependent impedance load with a small time delay. The delay used in this case was 0.1 millisecond. At switching instant, there is a drop in the real and reactive power because the impedance of the load is equal to the pre-contingency impedance value. This impedance is changed at the time step following the switching. The real and reactive powers recover to their nominal values but cannot be maintained constant around 0.445 seconds. This is because the low voltage at the load bus is insufficient to maintain a constant power load and experiences a collapse. As seen from Figure 5.41, the load bus phase angle shows large oscillations confirming the phasor assumption is violated. The generator bus voltage does not collapse and it seems to settle down near 0.6 pu.

Thus, it can be inferred that for a loading of P_d = 2.32 pu, the system does experience a transient voltage collapse with a constant power load at the load bus. This collapse is captured by modeling a constant power load as a voltage dependent impedance load model. Figures 5.43-5.44 show the response of the system at the loading level of P_d = 2.31 pu and 2.35 pu with the load modeled as a voltage dependent impedance load. Figure 5.43 shows that for a loading of P_d = 2.31, which is below the critical loading level of the system (P_d = 2.32 pu), the system survives the transient and settles down at a new steady state operating point. For a loading of 2.35 pu, the system experiences a voltage collapse at the load bus as shown in Figure 5.44.

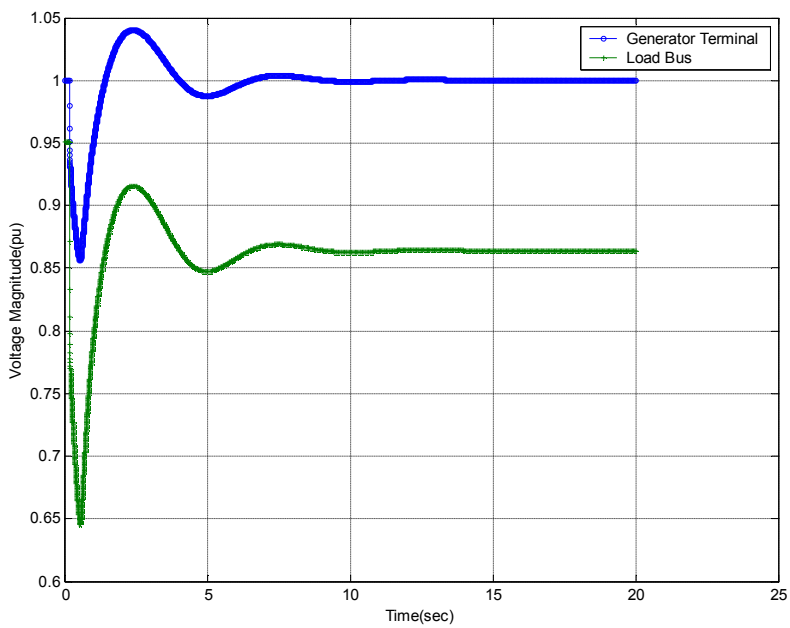

Figure 5.43 Generator and load bus voltage magnitude for P_d = 2.31 pu

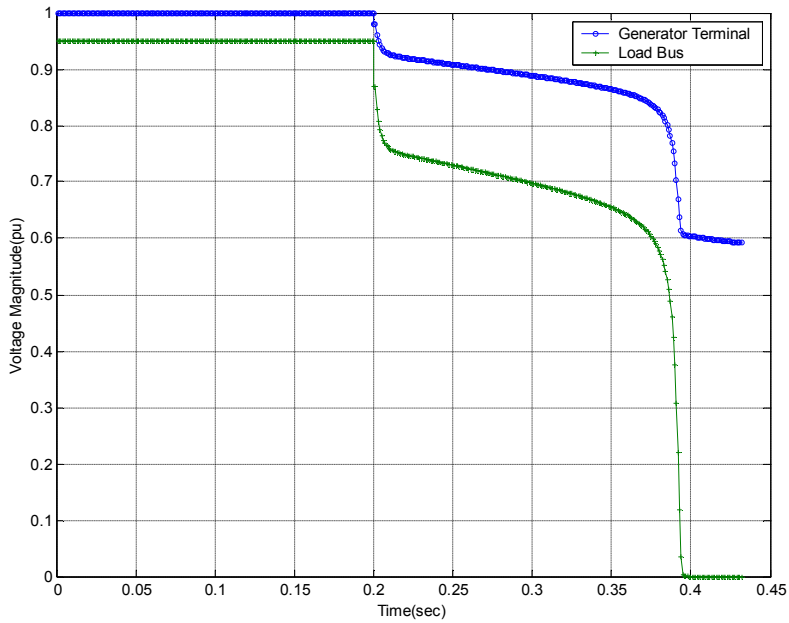

Figure 5.44 Collapse of the load bus voltage for $P_d = 2.35$ pu

5.6 Non-convergence of the transient stability simulation for constant power loads on switching

On increasing the load upto $P_d = 2.48$ pu, the transient stability simulation failed to converge at the switching instant. In the transient stability simulation, a one step solution of the algebraic system in the DAE model is carried out to compute the instantaneous response of the network on switching. This one step solution did not converge at the switching instant

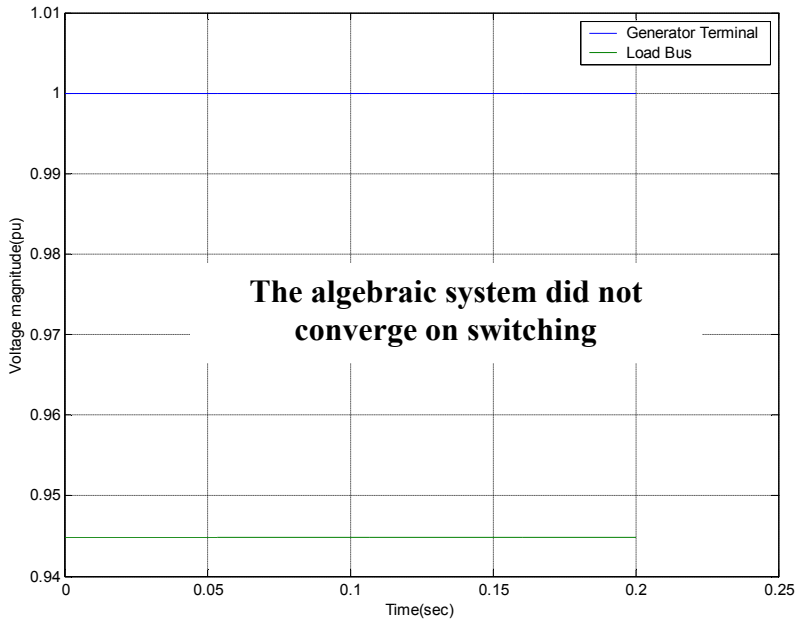

Figure 5.45 Non-convergence of the algebraic simulation at switching for $P_d = 2.48$ pu

To investigate this non-convergence, a continuation power flow, with only one line in service, was run with the generator modeled with the internal voltage source as given in Figure 5.46. This is the same internal voltage source as used for the stator algebraic equations and is also shown in Figure 3.1

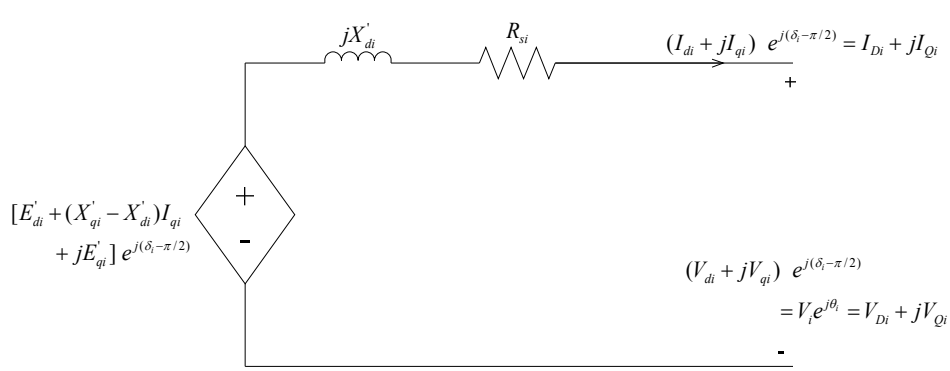

Figure 5.46 Interface of the generator terminal voltage and the internal voltage source of the generator

The internal voltage source of the generator can be decomposed in two parts; the first one involving the dynamic state variables which does not change instantaneously on switching, the second consists of the algebraic variable I_q which changes on switching. Hence the internal voltage source of the generator changes instantaneously on switching.

For the continuation power flow, an internal voltage source corresponding to the post-switching solution for a loading of 2.47 pu was used and kept fixed. This loading was selected because beyond this loading, the algebraic system did not converge on switching. The continuation power flow plot for this simulation is shown in Figure 5.47.

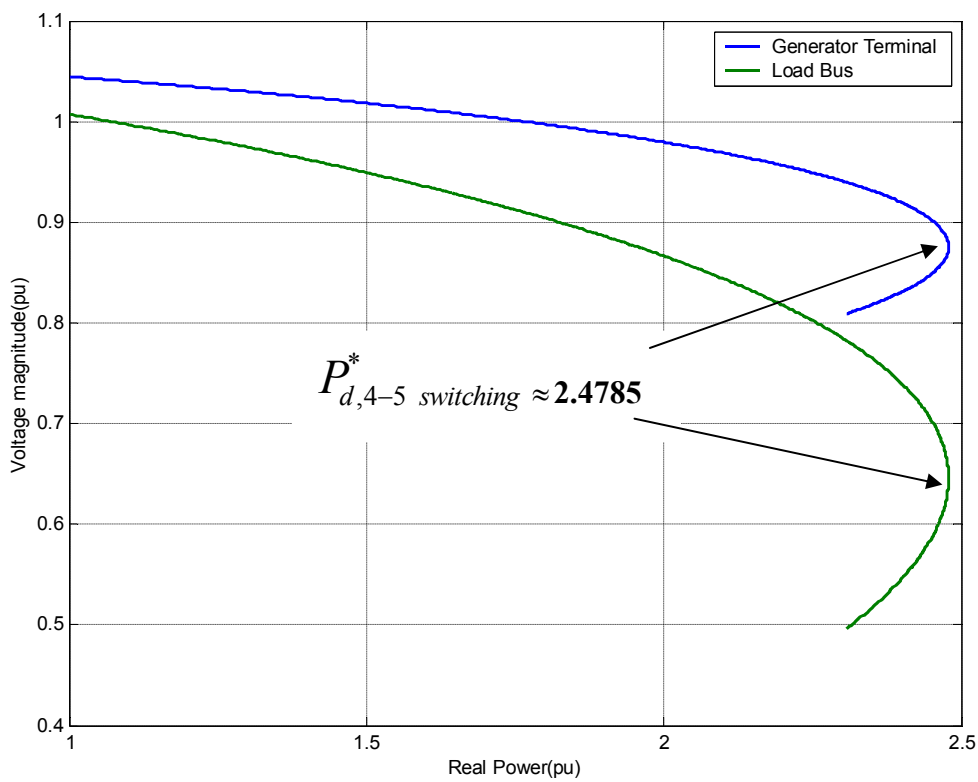

Figure 5.47 Continuation power flow plot with the internal voltage source of the generator fixed

As seen from Figure 5.47, the nose point for the continuation power flow curve is about 2.4785 pu which is less than 2.48 pu, the loading at which the transient stability simulation stops on switching. Thus, when a line is tripped at the loading level of 2.48 pu, the system is operating beyond the collapse and hence the transient stability simulation fails to converge on switching.

5.7 Conclusions

The conclusion of the results from this chapter can be summarized as follows:

- Results on the two bus system with constant voltage source and voltage dependent impedance load show that instantaneous time domain simulation can capture the voltage collapse beyond the steady state loading limit. The results agree with the continuation power flow.
- The voltage collapse can be also captured using a lumped parameter line instead of a distributed parameter line in instantaneous time domain simulation. Thus, voltage collapse can be captured even if an instantaneous network response is assumed.
- At or beyond voltage collapse conditions, the phasor assumption loses its validity.
- Simulations in three phase instantaneous time domain show that at the critical loading limit of 2.32 pu, the system recovers for a balanced three phase star connected load.
- Implementation of the voltage dependent impedance load in the transient stability simulations show that such a load model captures the voltage collapse trajectories. By varying the load response time in the transient stability

simulation, it was found that the balanced three phase voltage dependent impedance was responding to the change in the voltage approximately after half a cycle. By using a small delay (0.1 milliseconds), voltage collapse for constant power load could be closely followed too.

- The non-convergence of the transient stability simulations on switching is because immediately after switching, the operating point is beyond the loading limit for the system. This result is supported by the continuation power flow method.

CHAPTER 6

CONTRIBUTIONS AND FUTURE WORK

This thesis presented the transient analysis of power system with an aim of capturing the voltage collapse dynamics. The contributions of this thesis towards the target aimed are summarized below:

- Provided a new confirmation of the steady state voltage collapse via instantaneous time domain simulation
- Demonstrated that voltage collapse dynamics can be simulated accurately with both distributed and lumped parameter differential network models with voltage dependent impedance loads.
- Verified the weakening of the steady state phasor assumption under voltage collapse.
- Presented a thorough simulation of the two-bus, two-branch model in three - phase with a detailed generator model and voltage dependent impedance load.
- Proposed a crude strategy for tuning voltage dependent impedance loads in DAE Transient Stability Simulations to "match" the instantaneous behavior.
- Confirmed the failure mechanism of the DAE Transient Stability Simulation when post-switching solutions are not found with constant power loads.

Based on the results of this thesis and the associated work done, the future work can be visualized along the following lines:

- For capturing voltage collapses having slowly decaying characteristics, the transient stability simulations can be used. However, for non-convergence during the switching event, the instantaneous time domain simulation can be

used to guide the transient stability simulation. For large scale systems though, modeling the entire system in instantaneous time domain is inefficient. Thus, hybridization of the transient stability and instantaneous time domain simulation needs to be done to capture local and wide-spread voltage collapse. The hybrid concept involves modeling of most of the system using transient stability simulators and the critical part modeled in instantaneous time domain. Such a strategy is discussed in [13] for HVDC lines interfacing or for interfacing power electronic equipments with the network.

- The modeling of other power system equipments like tap-changing transformers, governors, different exciters, over excitation limiters, power system stabilizers, etc. need to be modeled to get a more realistic representation of the power system in the Transient Stability Simulations as well as the Instantaneous Time Domain Simulation.
- The voltage dependent impedance model has been tested on a two-bus system however, it needs to be tested on bigger systems and different transient scenarios. The response time of the voltage dependent impedance load is also a critical issue that needs to be investigated to get a better understanding of the load response. For a system in which the loads respond with different time delays, an efficient step size of the transient stability simulation needs to be determined to do a fast and accurate simulation.
- The distance to transient voltage collapse needs to be investigated for its prevention.

APPENDIX A

TWO BUS SYSTEM DATA

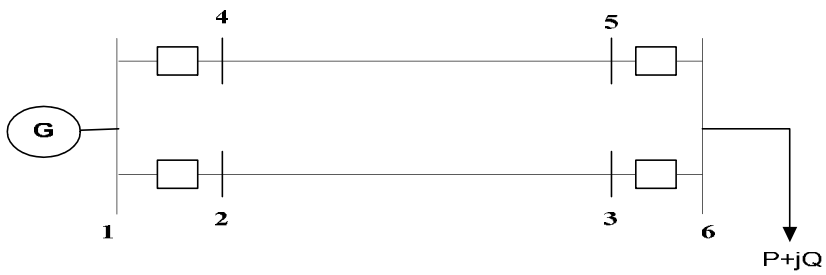

Figure A.1 Test system topology

Table A.1 Base case load flow results for the two bus system

	Bus #	Voltage(pu)	P_G (pu)	Q_G (pu)	$-P_L$ (pu)	$-Q_L$ (pu)
1	(swing)	$1.0\angle 0^o$	1.0047	0.00546	-	-
2	(P-Q)	$0.995\angle 0.002^o$	-	-	-	-
3	(P-Q)	$0.98628\angle -2.722^o$	-	-	-	-
4	(P-Q)	$0.995\angle 0.002^o$	-	-	-	-
5	(”)	$0.98628\angle -2.722^o$	-	-	-	-
6	(”)	$0.98578\angle -2.711^o$	-	-	1	0.35

Table A.2 Exciter data

Parameters	Value
K_A	20
T_A (sec)	0.2
K_E	1.0
T_E (sec)	0.314
K_F	0.063
T_F (sec)	0.35

Table A.3 Machine data

Parameters	Value
H (sec)	8.3
X_d (pu)	0.146
X'_d (pu)	0.0608
X_q (pu)	0.4360
X'_q (pu)	0.0969
T'_{do} (sec)	8.96
T'_{q0} (sec)	0.31
R_s (pu)	0.00576
D (pu)	2

Table A.4 Branch data

Branch	Resistance(pu)	Reactance(pu)	Susceptance(pu)
1-2	0.001	-	-
1-4	0.001	-	-
3-6	0.001	-	-
5-6	0.001	-	-
2-3	0.006822	0.094838	0.17538
4-5	0.006822	0.094838	0.17538

Table A.5 Transmission line distributed parameters

Branch	R' (per km.)	L' (per km.)	C' (per km.)	Line Length (km.)
2-3	.6861E-04	2.5226E-06	4.6454E-06	100
4-5	.6861E-04	2.5226E-06	4.6454E-06	100

BIBLIOGRAPHY

[1] Lachs, W. R., and D. Sutanto. "Different types of voltage instability." *IEEE Transactions on Power Systems*. 9 (May 1994): 1126-1134.

[2] Vournas, C. D., G. A. Manos, J. Kabouris, and T. V. Cutsem. "Analysis of voltage instability incident in the Greek power system." *IEEE Power Engineering Society Winter Meeting*. 2(23-27 Jan 2000): 1483-1488.

[3] Venikov, V. A., and M. N. Rozonov. "The stability of a load." *Izv. Akad. Nauk SSSR* (*Energetika I Artomatica*). 3 (1961): 121-125.

[4] Kwatny, H. G., A. K. Pasrija, and L. Y. Bahar. "Loss of steady state stability and voltage collapse in electric power systems." *Proceedings of IEEE Conference on Decision and Control*. Ft. Lauderdale, FL (Dec 1985): 804-811.

[5] Tamura, Y., H. Mori, and S. Iwamoto. "Relationship between voltage instability and multiple load flow solutions in electric power systems." *IEEE Transactions on Power Systems*. PAS-102 (May 1983):1115-1125.

[6] Ajjarapu, V., and C. Christy. "The continuation power flow: a tool for steady state voltage stability analysis." *IEEE Transactions on Power Systems*. 7 (Feb. 1992): 416-423.

[7] Chiang, H. D., A. Flueck, K. Shah, and N. Balu. "CPFLOW: A practical tool for tracing system steady state stationary behavior due to load and generation variations." *IEEE Transactions on Power Systems*. 10 (May 1995): 623-634.

[8] Kundur, P. *Power system stability and control*. New York: McGraw-Hill Inc., 1994.

[9] Dobson, I., H. -D. Chiang, J. S. Thorp, and L. Fekih-Ahmed. "A model of voltage collapse in electric power systems." *Proceedings of IEEE Conference on Decision and Control*. (1998): 2104-2109.

[10] Cutsem, T. V. "Voltage instability: phenomena, countermeasures and analysis methods." *Proceedings of the IEEE*. 88.2(Feb. 2000): 208-227.

[11] Huang, G. M., and N. C. Nair. "Detection of dynamic voltage collapse." *IEEE Power Engineering Society Summer Meeting*. 3 (2002): 1284-1289.

[12] Sauer, P.W., and M. A. Pai. *Power system dynamics and stability*. New Jersey: Prentice Hall Inc., 1998.

[13] Watson, N., and J. Arrillaga. *Power system electromagentic transients simulation*. London, UK: The Institution of Electrical Engineers, 2003.

[14] Zimmerman, R. D., and D. Gan. *MATPOWER version 2.0 user's manual*. Cornell University, Ithaca, New York: Power Systems Engineering Research Center, 1997.

[15] *Power System Blockset user's guide*, *version 1*. TEQSIM International Inc., 1999.

[16] Saadat, H. *Power system analysis*. New York: McGraw-Hill Inc., 1999.

[17] Dobson, I., H. Glavitsch., C-C. Liu., Y. Tamura and K. Vu. "Voltage collapse in power systems." *IEEE Circuits and Devices Magazine*. 8.3 (July 2003): 40-45.

[18] Flueck, A. J. *Advances in numerical analysis of nonlinear dynamical systems and the application to transfer capability of power systems*. Diss. Cornell University, 1996.

[19] Tirupati, V. *Integration of transient stability and relay co-ordination, and applications of branch admittance based continuation method*. MS thesis. Illinois Institute of Technology, 2004.

[20] Dobson, I., H. Glavitsch, C-C. Liu, Y. Tamura, and K. Vu. "Voltage collapse in power systems." *IEEE Circuits and Devices Magazine*. 8.3 (May 1992):40-45.

[21] Lee, B. H., and K. Y. Lee. "A study on voltage collapse mechanism in electric power systems." *IEEE Transactions on Power Systems*. 6 (Aug. 1991): 966-974.

[22] Srivastava, A. *Voltage collapse contingency screening and power grid vulnerabilities*. Diss. Illinois Institute of Technology, 2005.

[23] Ong C. *Dynamic simulation of electric machinery using MATLAB/SIMULINK*. Taiwan: Prentice Hall, 1994.